Photoinduced Electron Transfer at Molecule−Metal Interfaces

C. D. Lindstrom and X.-Y. Zhu*

Department of Chemistry, University of Minnesota, Minneapolis, Minnesota 55455

Received January 24, 2006 (Revised Manuscript Received July 31, 2006)

Contents

1. Introduction

Photoinduced electron transfer (ET) at molecule−metal or molecule−semiconductor interfaces is of interest to many research fields. Examples include, among others, photocatalysis,[1−3] surface photochemistry,[4−9] dye-sensitized solar cells (DSSCs),[10−12] organic semiconductor-based photovoltaics,[13,14] and nanoscale optoelectronics based on a single molecule or a small group of molecules.[15] Although this review focuses on molecule−metal interfaces, many of the concepts and conclusions apply equally well to molecule−semiconductor interfaces. Figure 1 illustrates the basic system

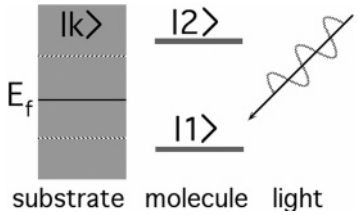

Figure 1. Schematic illustration of the interaction among light, molecular electronic states ($|1\rangle$ and $|2\rangle$), and electronic continuum ($|k\rangle$) in the metal or semiconductor substrate. E_f denotes the Fermi level. Dashed lines represent a possible band gap in the substrate.

common to all the examples above: discrete molecular electronic levels (e.g., $|1\rangle$ and $|2\rangle$) interacting with a continuum of electronic states ($|k\rangle$) in a metal or semiconductor substrate under the influence of a radiation field. Here, the molecular electronic levels may represent the highest occupied molecular orbital (HOMO) and the lowest unoccupied molecular orbital (LUMO). The substrate electronic continuum often contains gaps, e.g., projected bulk energy gaps in metals for particular crystallographic directions or electronic energy gaps integrated for all momentum spaces in semiconductors.

What are the physical processes involved in such a system? To answer this question, let us consider the total Hamiltonian:[15]

$$\hat{H} = \hat{H}_o + \hat{V} \quad (1)$$

$$\hat{H}_o = \hat{H}_M + \hat{H}_S + \hat{H}_P \quad (2)$$

$$\hat{V} = \hat{V}_{ET} + \hat{V}_{DC} + \hat{V}_{PM} + \hat{V}_{PS} + \hat{V}_{PMS} \quad (3)$$

where $\hat{H}_o$ is simply the sum of Hamiltonians for the isolated molecule ($\hat{H}_M$), substrate ($\hat{H}_S$), and radiation field ($\hat{H}_P$). $\hat{V}$ is the coupling term and contains all the physics of interest. It includes (i) electron-transfer coupling, $\hat{V}_{ET}$, between each molecular state and the substrate electronic continuum; (ii) dipole−induced-dipole (energy transfer) coupling, $\hat{V}_{DC}$, between an excited molecule and the dielectric response of the substrate; (iii) molecule−radiation field coupling, $\hat{V}_{PM}$; (iv) substrate−radiation field coupling, $\hat{V}_{PS}$; and (v) molecule−substrate−radiation field coupling, $\hat{V}_{PMS}$, i.e., direct optical excitation between the substrate electronic continuum and a molecular electronic state. The different coupling terms in eq 3 have been probed in various experiments in the past.

10.1021/cr0501689 CCC: $59.00
Published on Web 10/11/2006

Chad Lindstrom was born in 1974 in Vermillion, South Dakota, USA. He was a distinguished graduate from the U.S. Air Force Academy in 1996 with degrees in Math and Physics. He received a Master's Degree in electrical engineering from the University of Washington, Seattle. Subsequently, he worked for three years as an Air Force officer (research physicist) at the Air Force Research Laboratory at Kirtland AFB, New Mexico, and followed that assignment with two years as a physics instructor at the U.S. Air Force Academy. In 2002, he joined the group of Xiaoyang Zhu at the University of Minnesota and received his Ph.D. in Chemical Physics in 2006. His research interests include the study of metal–molecule interfaces with two-photon photoemission, nonlinear optics, laser development, laser spectroscopies, and signal processing/tomography. He will soon join the Air Force Research Laboratory, Wright-Patterson AFB, Ohio, to develop optical in-flight diagnostics of supersonic combustion ramjet engines.

Xiaoyang Zhu is a Professor of Chemistry at the University of Minnesota–Minneapolis. He obtained a B.S. degree in Chemistry from Fudan University in 1984 and a Ph.D. degree in Chemistry from the University of Texas at Austin in 1989. Following postdoctoral research at Austin and as a Humboldt fellow at the Fritz–Haber–Institute in Berlin, he joined Southern Illinois University as an Assistant Professor of Chemistry in 1993. He joined the Minnesota faculty in 1997, first as an associate professor and then professor of chemistry. His honors include a Dreyfus New Faculty Award, a Cottrell Scholar Award, and a Friedrich Wilhelm Bessel Award. His research interests are in the area of surface and interfacial sciences, including interfacial electron transfer, molecular electronics, solar energy conversion, biointerfaces, nanomechanics, and biophysics.

The electron-transfer coupling term, $\hat{V}_{ET}$, measures the electronic interaction between a discrete molecular state and the substrate continuum. In the simplest case, where elastic resonant electron transfer (RET) dominates, $\hat{V}_{ET}$ is responsible for the mixing of the discrete molecular level and the substrate continuum and results in a broadened molecular resonance whose width Γ is a direct measure of the electron-transfer rate or lifetime (τ), based on the Uncertainty Principle:

$$\Gamma \approx \frac{\hbar}{\tau} \tag{4}$$

This scenario is best-represented by the Newns−Anderson chemisorption theory,[16] but it becomes more complex when inelastic and Auger processes are operative for interfacial ET. Let us consider two examples where $\hat{V}_{ET}$ is important. The first example is a dye-sensitized solar cell (DSSC),[17] where the photon energy is sufficient to excite the adsorbed molecule via $\hat{V}_{PM}$ but not sufficient to excite the wide-band gap semiconductor substrate. In this case, $\hat{V}_{ET}$ determines the rate of electron injection (resonant electron transfer, RET) from the transiently occupied molecular state ($|2\rangle$) in the photoexcited molecule to the substrate conduction band. Back-electron transfer from the semiconductor to the molecule is not as important, because the photohole ($|1\rangle$) is usually located within the semiconductor band gap and less efficient inelastic or Auger processes are necessary for it to happen. The second example is photocatalysis or substrate-mediated surface photochemistry,[8,9] where optical excitation due to $\hat{V}_{PS}$ creates excited electrons/holes in the metal or semiconductor substrate. $\hat{V}_{ET}$ then determines the rate of electron or hole transfer to the adsorbed molecule, as well as that of the back transfer of charge from the transient anionic or cationic species to the substrate. Note that the $\hat{V}_{ET}$ terms differ in the two examples that were illustrated previously. In a dye-sensitized photovoltaic, one has a charge-neutral excited molecule and electron injection occurs in the presence of the photohole on the molecule. In photocatalysis or substrate-mediated surface photochemistry, the opposite charge in the metal or semiconductor substrate is usually screened. As a result, electron or hole transfer to the molecule results in a transient anionic or cationic species.

The dipole−induced-dipole coupling between a photoexcited molecule and the substrate is equivalent to Foerster energy transfer in molecular photophysics. Classical electromagnetic descriptions of the energy transfer rate, as a function of molecule−surface distance, particularly by the work of Chance, Prock, and Silbey,[18] have shown excellent agreement with experimental measurements of fluorescence lifetimes on both metal and semiconductor surfaces.[19,20] Such a classical description works well for molecules not in direct chemical interaction with the solid surface. In the case of strong chemisorption systems, the rate of ET is usually believed to be much higher than that of energy transfer. As a result, energy transfer is regarded as a minor competitive pathway.

Although optical excitation of the molecule ($\hat{V}_{PM}$) and the substrate ($\hat{V}_{PS}$) are both well-established mechanisms, much less is known about molecule−substrate−radiation field coupling ($\hat{V}_{PMS}$), i.e., direct photoinduced ET between the substrate and the adsorbed molecule. When electron-transfer coupling between a molecular orbital and the substrate electronic continuum is weak, one expects the transition dipole moment between the two to be small. As $\hat{V}_{ET}$ increases, we expect more and more wave function mixing

between the molecular level and substrate electronic bands. As a result, the transition dipole moment for a direct optical transition between a substrate state ($|k\rangle$) and a molecular state ($|1\rangle$ or $|2\rangle$) may no longer be small. This mechanism has received little attention in the literature on DSSC, photocatalysis, and surface photochemistry, but has been shown to be a dominant mechanism in recent experiments on two-photon photoemission (2PPE) spectroscopy of molecule−metal or molecule−semiconductor interfaces.[21,22] In a 2PPE experiment, an initial pump photon excites an electron from a surface or substrate state ($|k\rangle$) to an unoccupied molecular state ($|2\rangle$) which is then ionized by a second probe photon and detected by an electron energy analyzer (hole detection is obviously not possible in this approach except through indirect methods). Given the 2PPE results, it is likely that the traditional view of photoinduced electron-transfer in strongly coupled systems for DSSC and surface photochemistry should be modified to include the direct photoexcitation mechanism.

We must note that photoinduced charge transfer at molecule−metal or molecule−semiconductor interfaces is a problem for which the general concepts or theories such as eqs 1−3 exist; however, their specific applications to individual systems are very difficult at the present time. This is due to a combination of two factors: (i) the extended nature and reduced symmetry at the molecule−metal or molecule−semiconductor interface, and (ii) the difficulty in dealing with excited electronic states. Experiments must often lead the way in determining what factors determine the photoinduced charge-transfer rate. The goal of this account is to highlight the trends that have been observed in experimental studies and also the deficiencies in our current understanding of photoinduced charge transfer at metal−molecule interfaces. In particular, our objective is to promote a closer interaction between theories and experiments. The key question is: given a molecule/metal system, what determines that rate of photoinduced ET? The emphasis here is on qualitative predictions, instead of quantitative interpretations of experimental data. In the following, we first present concepts and theories (often borrowed from molecular and solid-state physics) that are important to photoinduced ET. This is followed by a detailed discussion of experimental studies that have probed different aspects of photoinduced ET at molecule−metal interfaces.

2. Theory

The ingredients for understanding photoinduced interfacial charge transfer can be found in several different fields, including molecular photophysics,[23] surface photochemistry,[4−9] photoemission spectrocopies (one- and two-photon),[24−27] electronic structure theory,[28−31] and charge transport in molecular junctions.[32] The process can be divided into two primary mechanisms: direct and indirect. The direct mechanism involves photoexcitation from a bulk metal or surface state ($|k\rangle$) to a molecular state ($|2\rangle$) that can be described using matrix elements from $\hat{V}_{PMS}$ in eq 3. An analogous process is the direct photoexcitation from a molecular state ($|1\rangle$) to a substrate state ($|k\rangle$) that might be operative in DSSC. The indirect mechanism involves initial photoexcitation of the substrate or the molecule, followed by interfacial ET, as determined by $\hat{V}_{ET}$. If the initial excitation occurs in the molecule ($\hat{V}_{PM}$), the excited electron in $|2\rangle$ can rapidly decay into the vast number of unoccupied substrate states; this is the electron injection problem in DSSC.[17] If the initial excitation is in the substrate ($\hat{V}_{PS}$), interfacial ET results in the attachment of an excited electron or hole to the molecule; this is essentially substrate-mediated surface photochemistry.[8,9] A variation of the previously described picture is found in photocatalysis, where interfacial ET occurs between a surface trapped charge or exciton and a molecule.[1−3]

This review focuses on two factors that are probed in experiments: $\hat{V}_{ET}$ and $\hat{V}_{PMS}$. The former determines the rate of ET between a photoexcited substrate and the molecule (or vice versa) and the latter corresponds to direct photoinduced interfacial ET. We begin with a brief discussion on what constitutes the initial and the excited state (i.e., electronic structure), including a brief overview of the essential elements of band structure theory and what happens to molecular orbitals upon chemisorption. Emphasis is next given to the symmetry of the molecule and the metal surface in the context of the direct photoinduced electron-transfer mechanism. We also consider other key factors that influence the direct mechanism. We then address the indirect mechanism for the case of the attachment of a photoexcited substrate electron to a molecule. Here, we highlight the recent work of Nakamura and Yamashita,[33] using the nonequilibrium Green's function approach to describe the hot-electron attachment process, because it is a useful attempt in bridging the gap between photoinduced charge transfer and charge transport theories. We then address the decay dynamics of a transiently populated molecular resonance from time-resolved 2PPE and other complementary experiments. Finally, we discuss the difficult problem of electronic−nuclear coupling and dynamic localization in photoinduced interfacial ET.

2.1. Electronic Structure

2.1.1. The Metal Surface

A prerequisite to understanding much of the latter discussion depends on understanding metal surfaces which possess some common properties. A brief overview of metal surfaces,[34] with specific emphasis on the (111) faces of noble metals, is given below. Next, the case of physisorption is considered and its effects on the affinity level of the adsorbate will be examined. Finally, key concepts of chemisorption will be examined.

When one views along a particular direction in a metal, one may find gaps in its band structure, as illustrated in Figure 2; this is called a projected band gap. Here, the bulk band structure along the [111] direction of a noble metal is depicted, where $\mathbf{k}_\perp$ is a reciprocal lattice vector perpendicular to the (111) surface. The presence of the surface means $\mathbf{k}_\perp$ is not conserved at the surface. However, $\mathbf{k}_\parallel$ in the plane of the surface is conserved for single-crystal surfaces and for ordered adsorbate layers commensurate with the underlying substrate. As one moves to different values of $\mathbf{k}_\parallel$, the band edges, as well as the surface states, disperse. The first important consequence of this gap is that states localized at the surface are formed in the gap consisting of Bloch-like wave functions that decay into the bulk and match decaying wave functions into the vacuum.[35] The probability density of the surface state (SS) is peaked at the metal surface. Thus, resonant photoexcitation from SS to adsorbate states becomes possible. In the following, we will use the words "state" and "resonance"; a distinction between the two lies in its energetic location, with respect to the substrate band gap. A state is located within a bulk-projected band gap and its probability

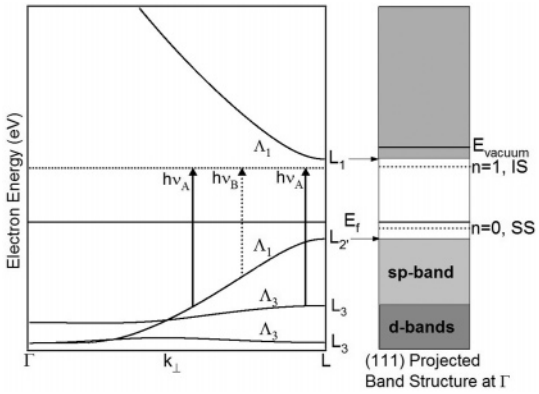

Figure 2. Projection of the bulk band structure at the center of the surface Brillouin zone (SBZ) for the (111) face of a noble metal, along with the symmetry labels for the bulk bands. The $n = 1$ image state and the $n = 0$ surface state are shown. The solid arrow shows possible transitions at wavelength, $\hbar v_A$, and the dashed arrow shows possible transitions at wavelength, $\hbar v_B$, to the $n = 1$ image state.

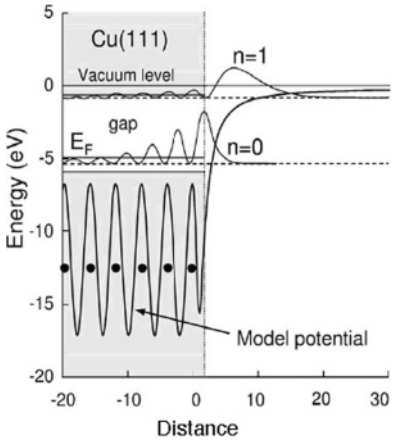

Figure 3. One-dimensional (1D) model potential and probability density for the intrinsic surface state ($n = 0$) and the first image-potential state ($n = 1$) at the Cu(111) surface at $\bar{\Gamma}$. Reprinted with permission from *Surf. Sci. Rep.*, ref 39. Copyright 2004 Elsevier.

density decays exponentially into the bulk of the metal. A resonance is located within a bulk band and is energetically resonant with continuum states of the metal substrate.

Another type of state that can transfer charge out of the bulk and into or beyond a molecular layer is an image state. An image state is formed from an electron trapped in the potential well that is created between the image potential and the projected band gap.[36−39] Figure 3 shows a one-dimensional model potential proposed by Chulkov and co-workers that has been used to accurately describe the decay dynamics of image states at the surface of copper and silver.[40,41] Notice here that the projected band gap is approximated by a cosine function, whose Fourier coefficient determines the band gap in the usual two-band formulation. The model potential varies smoothly from the bulk to the classical image potential on the vacuum side, as given by

$$V_{\mathrm{im}} = -\frac{1}{4\pi\epsilon_{\mathrm{vac}}}\left[\frac{e^2}{4(z - z_{\mathrm{im}})\epsilon_{\mathrm{s}}}\right] \tag{5}$$

where z_{im} is the static image-plane position, ϵ_{s} the dielectric constant of the adsorbate layer ($\epsilon_{\mathrm{s}} = 1$ for vacuum), and ϵ_{o} the vacuum permittivity. The image potential results in a Rydberg-like sequence of energy levels:[36−39]

$$E_n = \frac{-0.85\ \mathrm{eV}}{(n + a)^2} \tag{6}$$

where E_n represents the energy relative to the vacuum level ($n = 1, 2, ...$) and a is the quantum defect parameter, which is related to the phase shift experienced by the image electron as it reflects off the surface, because of the projected band gap. Figure 3 illustrates that the probability density of image states are located mostly outside of the metal. They are confined perpendicular to the surface but disperse as free electrons parallel to the surface. In comparison, the surface state overlaps strongly with the bulk and its dispersion depends on its interaction with the crystal. Image states are well-known for low-index noble-metal surfaces,[39−42] as well as those with molecular adsorbates.[43] It has also been suggested that image states may act as efficient conduits for charge transport at the surface if they are energetically close to molecular resonances that are present at the interface.[44−46]

2.1.2. Physisorption

Physisorption of a molecule on a metal surface occurs via van der Waals or dispersion forces.[34] The primary distinction of physisorption from chemisorption is that there is little hybridization of molecular orbitals with the metal in the former. Consider the simplest case of a rare gas atom on a metal surface. The valence electron distribution in the atom is polarized toward the metal surface because of two forces: (i) the classical image force (eq 5) and (ii) the quantum mechanical exchange-correlation force. The latter results from the fact that electrons prefer to stay away from each other, because of the Pauli exclusion principle; in other words, each electron is associated with an exchange-correlation hole. A valence electron on the atomic adsorbate has the lowest energy near the metal surface, because it is attracted by the image charge and because it is surrounded the most by the exchange-correlation hole. At the closest distance, exchange-correlation repulsion between the atomic valance electrons and the spill-out electron distribution from the metal substrate starts to dominate. The combination of the attractive interaction and the repulsive interaction leads to a shallow potential well a few angstroms from the surface. Note that polarization of the adsorbate valence electron distribution is accompanied by redistribution of surface electron density of the metal. In particular, the spill-out electron density is pushed back into the metal substrate. The decrease in the metal surface dipole moment and the addition of an adsorbate dipole moment (due to the polarized adsorbate electron distribution) both serve to lower the work function of the surface.

The effect of physisorption on photoinduced interfacial ET can be realized mainly in terms of the energetic position of molecular states/resonances, as a function of the distance to the metal surface. Take the LUMO of a physisorbed molecule as an example. ET from the metal substrate to the LUMO leads to the formation of a transient molecular anion. The anionic state/resonance is stabilized by the electrostatic potential associated with the physisorption well. If the electron density distribution of the anionic state/resonance

is peaked at more than a few angstroms (~3 Å) from the metal surface, its stabilization is dominated by contribution from the image potential and one can estimate the distance dependence of the electron affinity, based on eq 5. In particular, the vertical electron affinity level, with respect to the Fermi Level, can be approximated by

$$E_{-}(z) = \Phi - A - \frac{1}{4\pi\epsilon_{vac}} \frac{e^2}{4(z - z_{im})\epsilon_s} - E_{pol} \quad (7)$$

where Φ is the surface work function, A the vertical gas-phase electron affinity, and E_{pol} the polarization interaction with surrounding adsorbates. Notice that, in this case, the electron affinity level is effectively pinned to the vacuum level, not the Fermi level, because of its dependence on the work function. This has been demonstrated in inverse photoemission studies, such as benzene on different noble metal surfaces.[47] The image potential pulls the adsorbate electron affinity level down, and, therefore, it is possible that the electron affinity moves from above the vacuum level far from the surface to below the vacuum level near the surface, as shown for molecules such as benzene and naphthalene on Ag(111).[48] It is important to note that eq 7 is an approximation, because it is not a point charge with which we are concerned. The excess electron in the anionic state/resonance for a polyatomic molecule is distributed throughout the molecule. Take polyacene as an example. As the size of the molecule increases, the extra electron added to form the anion is spread over a larger space, because of the delocalized nature of the LUMO; as a result, the amount of stabilization by the image potential decreases as the molecular size increases. Finally, the last term of eq 7, E_{pol}, is often approximated from the bulk dielectric susceptibility of condensed phase molecules; this is a crude approximation for thin films. More refined approaches such as that used by Marinica and co-workers is needed to describe the situation accurately.[49]

Even for a physisorbed molecule, virtual orbitals such as LUMO + n (n = 0, 1, 2, ...) that are not involved in the physisorption process can still be strongly coupled to the metal surface through extensive wave function mixing. Photoinduced ET (direct or indirect) involving these virtual orbitals can occur with ultrafast rates.

2.1.3. Chemisorption

In contrast to physisorption, chemisorption involves significant interaction between the adsorbate and the substrate so that hybridization occurs.[28−31] Here, we give an overview of what occurs, based on the Newns-Anderson model,[16] which is similar to the Wigner−Weisskopf model used in optical and nuclear physics.[50,51] In this model, a single adsorbate level, $|a\rangle$, interacts with a continuum of Bloch states, $|k\rangle$, in the substrate and the goal is to describe how this affects the adsorbate level. In this simple model, the shift of the adsorbate level due to the image interaction described previously has been neglected. Consider eqs 1−3. In the absence of radiation field and the energy transfer coupling term, the Hamiltonian reduces to

$$\hat{H} = \hat{H}_M + \hat{H}_S + \hat{V}_{ET} \quad (8)$$

where the electron-transfer coupling term is responsible for the broadening of the molecular resonance. In the simplest case, where the molecule−metal interaction energy is smaller than the width of the metal band, which can be approximated by a constant density of states (Figure 4), the projected density of mixed states onto the original adsorbate level has a Lorentzian shape, with the width Γ given by

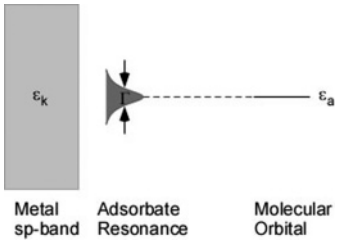

Figure 4. Schematic of weak chemisorption with sp-band metal.

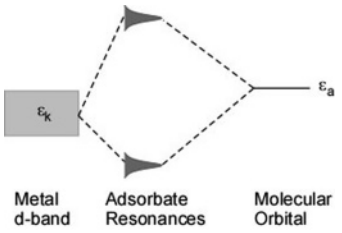

Figure 5. Schematic of the strong chemisorption due to interaction with the metal d-band.

$$\Gamma(E) = \pi \sum_k |V_{ET}(k)|^2 \delta(E - \epsilon_k) \quad (9)$$

This means that the adsorbate level is broadened into a resonance centered around ϵ_a. Thus, lifetime of the transient molecular resonance from a time-resolved experiment is a quantitative measure of Γ, based on eq 4.

In the case of strong chemisorption, with the interaction energy V_{ET} larger than the bandwidth of the metal, the adsorbate state splits to a bonding and an antibonding state (see Figure 5). This occurs with metals that have narrow d-bands, such as transition and noble metals. The rates of ET into or out of these molecular states/resonances are still related to electronic-coupling strength but a simple relationship such as eq 4 does not exist in this case.

2.2. Direct Photoinduced Electron Transfer

The direct photoexcitation channel is schematically depicted in Figure 6. The electron is photoinjected via the usual dipole transition, so the photoinjection rate is

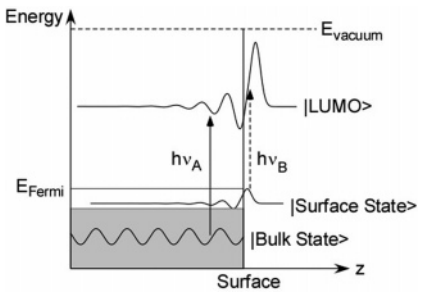

Figure 6. Schematic illustration of the direct optical excitation process to an unoccupied molecular resonance at the surface that proceeds either from bulk states or from surface states; the two paths are resonant at different photon energies. A third path from an occupied molecular orbital is also possible but does not constitute charge transfer from the metal. It is also possible to excite resonances above the vacuum level, but they then can also decay into the vacuum as well as the metal.

proportional to the transition dipole moment and light intensity if coherence between the initial and anionic state is ignored:[53]

$$R_{k2} \propto |\langle 2|\vec{\mu}|k\rangle \cdot \vec{E}|^2 \delta(E_2 - E_k - \hbar\omega) = |M_{k2}|^2 \delta(E_2 - E_k - \hbar\omega) \quad (10)$$

where R_{k2} is the rate of electron injection and $\langle 2|$ represents the unoccupied molecular state; $|k\rangle$ is the initial metal state, $\boldsymbol{E}$ is the electric field vector, and μ represents the transition dipole operator, which is often taken to be along a Cartesian axis (x, y, or z). A caution is necessary, because it is known from the photoemission of metal surfaces such as Al(100) that, at photon energies approaching the bulk plasma energy (~15 eV), the dipole approximation breaks down, because of rapid variations in the field perpendicular to the surface.[54,55] Because the plasma energy is typically much higher than the photon energy of interest in photoinduced charge transfer, we continue to use the dipole approximation. Equation 10 can be easily generalized to the case of multiple initial states that do not interact, to

$$T_2(\hbar\omega) = \sum_k R_{k2}(\hbar\omega) = \sum_k |M_{k2}|^2 \delta(E_2 - E_k - \hbar\omega) \quad (11)$$

where T_2 is the total photoinjection rate into state $\langle 2|$. This equation is innocuously simple looking, but quite complex in reality, because it requires knowledge of the wave functions involved. An examination of eq 10 or Figure 6 reveals two factors: (i) energy conservation and (ii) symmetry and spatial overlap of the wave functions that determines M_{k2}. We focus on the second factor in the following.

The discussion presented here pertains to photoinduced metal-to-molecule ET, i.e., $\langle k|$ being an occupied metal state and $|2\rangle$ an unoccupied molecule state (e.g., LUMO). The treatment applies equally to photoinduced molecule-to-solid ET, where $\langle 1|$ is an occupied molecule state (e.g., HOMO) and $|k\rangle$ is an unoccupied solid state (e.g., the conduction band of a semiconductor).

2.2.1. Optical Selection Rules and Space Groups

Similar to atoms or molecules, optical excitation at the surface must obey certain symmetry selection rules. Because we are examining a crystalline solid, the states overlap and form bands in the bulk, as well as at the surface, if the adsorbates possess long-range order. This requires inclusion of translational symmetry, which leads to Bloch's theorem with the point group symmetry that restores the lattice to itself. It is necessary to label the representations of a space group through the reduced wave vector, $\boldsymbol{k}$, and the irreducible representation of the group of that wave vector called its small representation.[56] Tables 1 and 2 illustrate the point groups associated with the band structure shown in Figure 2, along with the notation used in solid-state physics.[57]

Another important aspect concerns the reduction of symmetry upon adsorption of the molecule on the substrate.[58] Here, we use the aforementioned group tables to demonstrate this for a molecule such as BF_3 that possesses D_{3h} symmetry in the gas phase. Upon adsorption the horizontal mirror plane clearly is no longer a symmetry operation. So, the symmetry is reduced at least to C_{3v}, depending on the substrate. This means, for example, that orbitals belonging to the irreducible representations A_1' and A_1'' in D_{3h} go to A_1 in C_{3v}, as can be seen by comparing the columns of the common symmetry operations in Tables 1 and 2. Also note that the strength and type of interaction between the molecule and the substrate, as well as molecule−molecule interaction, determine the degree to which the symmetry decreases. For example, it is known that photoemission from the doubly degenerate 1π occupied orbital in the case of CO adsorbed on the (110) face of face-centered cubic (fcc) metal surfaces does not show splitting into its b_1 and b_2 components, despite the maximum symmetry of the surface being C_{2v}.[59] It is not just the adsorbate geometry that dictates the symmetry of the molecular states at the surface; geometry should only be taken as a starting point in a symmetry analysis. Nevertheless, symmetry selection rules have played an important part in the analysis of ultraviolet photoemission (UPS) and near edge X-ray absorption fine structure (NEXAFS) for molecules adsorbed at metal surfaces.[24]

Table 1. Characters for C_{3v} (Λ)

C_{3v} (Λ)	E	$2C_3$	$3\sigma_v$	basis
$\Lambda 1$, A_1	1	1	1	z
Λ_2, A_2	1	1	−1	R_z
Λ_3, E	2	−1	0	$(x,y)(R_x,R_y)$

Table 2. Characters for D_{3h} (L)

D_{3h} (L)	**E**	**$2C_3$**	$3C_2$	σ_h	$2S_3$	**$3\sigma_v$**	basis
L_1, A_1'	**1**	**1**	1	1	1	**1**	
L_2, A_2'	**1**	**1**	−1	1	1	**−1**	R_z
L_3, E′	**2**	**−1**	0	2	−1	**0**	(x,y)
L_1', A_1''	**1**	**1**	1	−1	−1	**−1**	
L_2', A_2''	**1**	**1**	−1	−1	−1	**1**	z
L_3', E″	**2**	**−1**	0	−2	1	**0**	(R_x,R_y)

The consideration of local symmetry, when combined with an understanding of space groups, provides a prescription for determining what bulk states are symmetry-allowed to contribute to the direct photoinduced electron-transfer process, in the case of an ordered adsorbate layer:

(1) Pick a reduced wave vector $\boldsymbol{k}_{||}$; this determines the direction in which the bulk bands are projected, e.g., $\boldsymbol{k}_{||} = 0$ for the noble metals in Figure 2.

(2) Determine which band(s) can energetically contribute to the photoemission process in which the unoccupied state energy is fixed in the $k_\perp$ direction. This is depicted for the $n = 1$ image state in Figure 2. In this case, the $\hbar\nu_A$ associates the image state with bulk bands of Λ_1 and Λ_3 symmetry, whereas $\hbar\nu_B$ only associates the image state to bands of Λ_1 symmetry. It may be necessary to consider backfolding of the bulk bands, because of an adsorbate superlattice.[24]

(3) Find the irreducible representations for those bands that are energetically allowed, taking into account the reduction in symmetry that is due to the surface. Continuing with the example, at the fcc surface, the irreducible representations are Λ_1 (A_1) and Λ_3 (E) for the bands of interest from Table 1. Now consider the irreducible representations for the unoccupied state and the dipole operator. Here, the image state is symmetric about the surface normal and is Λ_1 (A_1) and the dipole operator can be obtained from the basis column of Table 1 (z is Λ_1 (A_1) and x and y are Λ_3 (E)).

(4) Finally, multiply the irreducible representation characters of each band by the characters corresponding to the unoccupied molecular state and the dipole operator.

One can then determine if the totally symmetric representation is present in the result. This can be done using the following formula:

$$\frac{1}{m}\sum_{C} g(\mathrm{C})\chi(\mathrm{C}) \tag{12}$$

where m is the total number of operations in the group (i.e., $1 + 2 + 3 = 6$ for C_{3v}), g(C) is the number of operations in class C, and χ(C) is the character resulting from the multiplication described previously for class C. For example, for $\hbar\nu_B$ in Figure 2, the initial state must be A_1 and the final state is A_1; thus, for a field polarized in the z-direction, eq 12 gives a value of 1 whereas for fields polarized in the x- or y-directions it gives a value of 0. In contrast, for $\hbar\nu_A$, the polarization along the x- and y-directions are allowed transitions from the states with E symmetry, but the z-polarization is not allowed.

A similar procedure exists for transitions from surface states and occupied molecular states; however, in this case, one does not need to be concerned with the $k_\perp$ direction, because these states do not disperse in the vertical direction.

The rules previously listed seem to be straightforward to apply; however, their applications are often not possible, because the details of adsorption are usually unknown. At present, selection rules are not very useful, in terms of predicting whether direct photoinduced ET will occur for a particular metal−molecule system. Instead, they are better-employed post facto to help aid in the assignment of spectra to specific molecular orbitals. Finally, if we consider the dipole matrix element, the symmetry selection rules are clearly dependent on the polarization direction of the incident light, and, thus, the direct photoinduced ET rate can be controlled experimentally by varying the incident light polarization.

2.2.2. Spatial Co-localization of Wavefunctions

Spatial co-localization of wave functions most often determines whether the direct photoinduced ET channel is observed or not. Unlike the previous symmetry argument, no general procedures exist to determine this, and so it is necessary to consider the system on a case-by-case basis. This means numerical approximations to the wave functions must be found. Unfortunately, to the authors' knowledge, little work beyond image states at metal interfaces has been conducted in this direction. In the following, we present a qualitative discussion.

The initial metal wave function and the molecular wave function must co-localize in the same spatial region for the transition dipole moment (M_{k2} in eq 10) to be nonzero. In the case of image states, a strong correlation between the penetration of the tail of the image state wave function into the substrate and the photoexcitation cross section was observed.[60,61] Klamroth et al.[60] showed, using the model potential in Figure 3, that the matrix element, M_{k2}, scales with $(n + a)^{-3/2}$, whereas the probability density of the penetration of the wave function scales with $(n + a)^{-3}$. The high probability of photoinduced ET from bulk or surface states of the metal substrate to the image state is due to the fact that the image state is delocalized in the direction parallel to the surface.

For most molecules, an anionic molecular resonance/state is often localized to an individual molecule; as a result, its matrix element with delocalized substrate or surface bands must be vanishingly small and direct photoinduced ET does not occur. This may be the reason it is rare to observe anionic molecular resonances in 2PPE measurements. The matrix element for direct optical transition from a delocalized substrate state to a molecular level can be significant only when the molecular resonance/state of interest (i) mixes significantly with the metal substrate through strong chemical interaction, (ii) mixes with delocalized interface states (e.g., image states), or (iii) possesses parallel dispersion due to strong intermolecular electronic interaction and band formation. These three scenarios will be illustrated by selected examples in section 4. Note that, unlike the direct photoexcitation process that is important in a 2PPE process, population of a localized molecular state/resonance can easily occur via scattering. Indeed, evidence for anionic molecular state/resonance on surfaces is abundant in electron-adsorbate scattering, such as that in inverse photoemission spectroscopy, resonant electron stimulated desorption, and substrate-mediated surface photochemistry, as we discuss later.

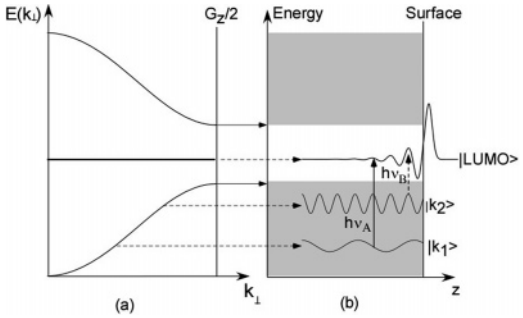

Figure 7. Schematic illustration of how the matrix element can be dependent on photon energy for excitation from a sp-band metal: (a) the perpendicular band structure and the positions of the Bloch states; (b) the real parts of the approximate wave functions used in the text as a function of z. The higher-energy state $|k_2\rangle$ more closely matches the spatial frequency of the |LUMO⟩ state and, therefore, has a higher cross section than the lower-energy state $|k_1\rangle$.

When significant electronic coupling between the molecule and metal substrate occurs and the resulting wave function penetrates into the metal, one can qualitatively estimate the rate of the direct photoinduced ET channel based on the match in spatial oscillations of the wave functions, as illustrated in Figure 7. Here, the optical transition matrix element is a strong function of the excitation photon energy due to differences in the spatial oscillation of the wave functions involved. A similar effect is well-known in UPS;[24] in this case, the final state energy determines the wave vector of the free electron and can be tuned by changing the photon energy. The same has been observed in the probe step in 2PPE.

Here, we show this effect using the image or surface state. In the simple two-band model of an almost free-electron metal, solutions exist in the gap that correspond to sinusoids damped into the bulk, as given by[39]

$$\psi_2(z) \propto e^{qz}\cos\left(\frac{1}{2}G_z z + \delta\right) \tag{13}$$

which is valid for $z < 0$ (i.e., in the substrate); q is the damping parameter determined by the energetic position in the gap ($q > 0$), G_z is the reciprocal lattice vector, and δ is

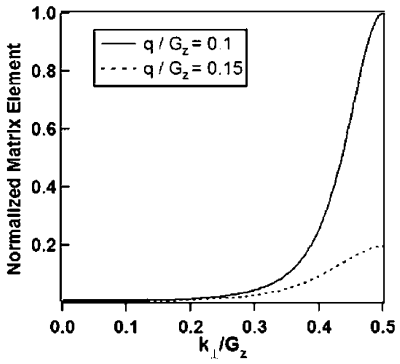

Figure 8. Matrix element of metal-to-image state optical transition for two different values of q/G_z, as a function of the reduced wavevector, $k_\perp/G_z$.

a phase shift that is also dependent on the position in the gap. We use this to model the tail of the wave function that penetrates into the substrate. For an initial state in the NFE model and if the wave vector is far from the zone boundary, the wave function can be approximated by a free-electron like state, $\psi_k(z) \propto e^{ikz}$. The matrix element then can be easily integrated (setting $\delta = 0$) for an optical field perpendicular to the surface, to give

$$|M_{k2}|^2 \propto \left| \frac{1}{\{q + i[k + (G_z/2)]\}^2} + \frac{1}{\{q + i[k - (G_z/2)]\}^2} \right|^2 \quad (14)$$

This expression, plotted in Figure 8, indicates two things: (i) the smaller q is, the larger the matrix element becomes, as expected from more penetration of the molecular state into the bulk; (ii) the closer the initial state vector k is to the zone boundary (i.e., $G_z/2$), the larger the matrix element. The latter indicates that the spatial frequencies of the initial and final state wave functions must be similar. This issue is not a symmetry selection rule, but it can explain relative differences between matrix elements. In particular, it emphasizes why charge transfer rates can be dramatically different for different photon energies, even though the density of states and symmetry of the initial states are similar.

2.2.3. Coherence in Direct Optical Excitation

The best evidence for direct optical excitation in photoinduced interfacial ET is the observation of coherent effects during photoexcitation. This is not the case when ET into the unoccupied molecular state occurs indirectly via scattering and loses phase information. The best example for coherent effects in photoinduced interfacial ET was shown by Hofer et al.,[62] for image states. These authors used ultrafast laser pulses with sufficiently large bandwidth to coherently excite a wave packet of closely spaced energy eigenstates ($n \geq 3$) of the image potential. This led to the observation of quantum beats among the excited image states. The adsorption of a molecular layer is observed to increase the dephasing rate and reduce the magnitude of quantum beats significantly, as shown by Reuss et al. for CO adsorption on the Cu(100) surface (see Figure 9).[63] Coherence for ET into molecular states/resonances is usually neglected, because dephasing is expected to be much faster. Petek and co-workers observed a small but measurable dephasing rate for photoinduced ET into the antibonding resonance for Cs−Cu(111).[64] Whether unoccupied states/resonance of polyatomic molecules at surfaces can exhibit measurable dephasing rates remains an open question.

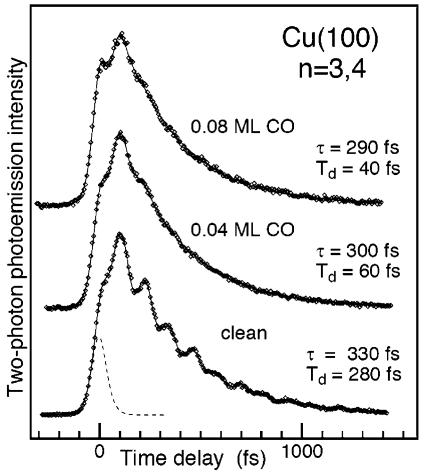

Figure 9. Quantum beats from the coherently excited $n = 3$ and 4 image states on Cu(100). The oscillations decay rapidly (T_d) upon CO adsorption, whereas the exponential decay representing the lifetime, τ, remains almost unchanged. The dashed line shows the cross correlation between pump and probe pulses. Reprinted with permission from *Phys. Rev. Lett.* (http://link.aps.org/abstract/PRL/v82/p153), ref 63. Copyright 1998 American Physical Society.

2.3. Photoinduced Indirect Electron Transfer

Indirect photoinduced ET at the metal−molecule interface most often involves the transfer of a hot electron in the metal substrate to the molecular state/resonance. In this process (shown in Figure 10), light absorption by the substrate creates a distribution of hot electrons. The hot electrons can travel to the surface and subsequently attach to the anionic state/resonance. Similarly, a hot hole in the metal substrate can attach to an occupied molecular state/resonance. The traditional view of electron injection in dye-sensitized solar cells can also be regarded as an indirect process where photoexcitation of the dye molecule and ET from the photoexcited dye molecule to the semiconductor conduction band are considered to be independent steps. For detailed descriptions of hot-electron dynamics on metal surfaces, we refer the readers to the excellent reviews of Petek and Ogawa[25] and Echenique et al.[39]

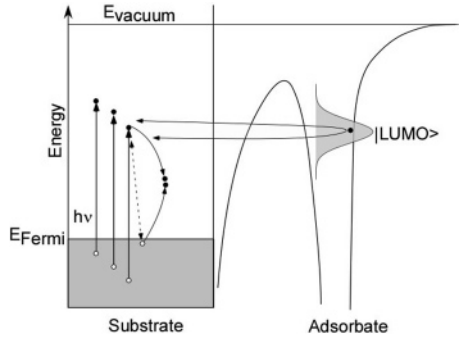

Figure 10. Schematic illustration of the hot-electron transfer to an unoccupied molecular resonance at the surface. The laser pulse generates hot electrons in the bulk, which scatter among themselves and also into the adsorbate level. The arrows inward and outward depict the idea of microscopic reversibility and also the possibility of inelastic processes that are occurring due to coupling to the nuclear degrees of freedom of the adsorbate.

2.3.1. Hot-Electron Transfer

The conceptual viewpoint of the hot electron-transfer process has already been given in Figure 10. Here, we focus on how hot-electron attachment rates can be determined. Phenomenological models that have been proposed by Gadzuk[6,65] have been used in the past to explain trends in hot-electron attachment rates, e.g., the photon energy dependence of photochemical cross sections.[66] However, for comparison among different adsorbate metal systems, these models are limited, because they use parametrized tunneling barriers to determine the cross section for the formation of the anionic resonance. A recent study by Nakamura and Yamashita allows for a first-principles treatment of the scattering problem at the surface and begins to provide a path toward more-predictive models.[33] In addition, it is constructed from the nonequilibrium Green's function (NEGF) formalism and provides a useful bridge to transport theories. These approaches are similar to the Berglund−Spicer model of photoemission.[67] The hot-electron attachment models divide the problem into three separate steps: (i) excitation of electrons in bulk; (ii) transport of excited electrons to the surface, including generation of secondary electrons through electron−electron scattering; and (3) tunneling of hot electrons into the unoccupied orbital. In both phenomenological and first-principles models, the first two steps are modeled in similar ways. However, the third step in the Nakamura and Yamashita model is very different from that of Gadzuk. This can be clearly seen by considering the resulting formulas for hot-electron attachment. First, we give the form from the phenomenological model:[65]

$$R(\omega) \propto \int_{E_F}^{E_F + \hbar\omega} f(E,\hbar\omega)T(E)e^{-(E_{aff} - E)^2/2s^2}\,dE \qquad (15)$$

where $f(E, \hbar\omega)$ is the hot-electron distribution at the surface created by the optical pulse and includes contributions from secondary electrons; $T(E)$ is the tunneling probability at energy E, determined by a simple potential barrier; and the third term corresponds to the energy broadening of the adsorbate affinity level. In contrast, the result of the Nakamura and Yamashita research is[33,68]

$$R(\omega) \propto \int_{E_F}^{E_F+\hbar\omega} dE\, \underbrace{\mathrm{Tr}\left[\Gamma_{eN}(E)G_c^R(E)\Gamma_{substrate}(E)G_C^A(E)\right]}_{\text{Similar purpose to } T(E)e^{-(E-E_F)^2/2s^2}} f(E,\hbar\omega)\theta(E-E_F) \qquad (16)$$

where $f(E, \hbar\omega)$ is the hot-electron distribution at the surface and is determined in a similar manner as in eq 15; $\theta(E - E_F)$ is the Heaviside step function; the highlighted term accounts for the attachment of hot electrons to the adsorbate affinity level. This formula can be compared to the NEGF formula for coherent transport in a metal−molecule−metal junction:[69]

$$I \propto \int \mathrm{Tr}[\Gamma_2(E)G_C^R(E)\Gamma_1(E)G_C^A(E)][f_2(E + \mathrm{eV}) - f_1(E)]\,dE \qquad (17)$$

where the f terms are the Fermi functions of the electrodes for a given bias voltage (V) across the junction and are analogous to the hot-electron distribution term $f(E, \hbar\omega)$ in eq 16. The first term, the transmission function through the junction, consists of four terms: $G_C^R(E)$ and $G_C^A(E)$ are the advanced and retarded Green's functions in the central region (i.e., the molecule + the nearest metal atoms) and describe coherent dynamics of the electron in this region; $\Gamma_1(E)$ describes the rate of electron injection into the central region from electrode 1, and $\Gamma_2(E)$ describes the rate of electron exiting the central region into electrode 2 (here, we have made the assumption that electrode current flows inward from electrode 1 and outward to lead 2). The Γ values here are due to the contact of the central region to the semi-infinite metal electrodes and account for lifetime broadening of molecular levels due to coupling to the metal; they are analogous to Γ in the Newns−Anderson chemisorption model, but they are matrixes instead of a single number. A key aspect of the transmission function in eq 17 is that all the constituents can be calculated from ab initio techniques: the Γ values are from surface Green's functions of the substrate[70−72] and can be calculated within the density functional theory (DFT), as is usually used in molecular conductance problems.[32,73−75]

The Green's function and the $\Gamma_{substrate}$ terms in eq 16 are similar to the respective terms in eq 17. The exception is Γ_{eN}, which describes the rate of attachment of electrons with some loss of electronic energy due to electronic−nuclear coupling responsible for vibrational excitation or chemical changes; it can be made sufficiently small to reach the quasi-elastic limit.

2.3.2. Interband and Intraband Scattering and Image-State-Assisted Scattering

There are other indirect channels for populating excited states at the interface. The mechanisms for these processes involve the excitation of an electron to a higher excited state or one of the same energy, followed by scattering into the unoccupied state of interest. If the rate of the scattering process is slow enough, it is possible to observe a finite rise time in the population dynamics that cannot be modeled with the optical Bloch equation or rate equation approach and it can affect the observed decay rate.[76−79] Evidence for these indirect channels comes from time- and angle-resolved two-photon photoemission, in which $k_{||}$-dependent decay rates are observed. The inelastic processes usually are associated with two effects at the interface: intraband electron−electron interactions and vibrational or rotational excitation of the molecule. The electron−electron interaction typically occurs on an ultrafast time-scale (i.e., tens of femtoseconds), but the vibrational or rotational excitations require a longer time. In the case of vibrational excitations of molecules, requirements similar to those of photochemistry or other desorption induced by electronic transitions (DIET) processes apply.[6] Examples for these indirect channels include intraband decay in cases of the LUMO band in C_6F_6 on Cu(111)[76] and image bands on metal surfaces[80] and interband decay processes from a higher-lying image state to a lower-image lying one.[26,81] There are also suggestions of unoccupied molecular states populated by decay from image states.[82] Finally, there is the case of image-state assisted tunneling of hot electrons from the bulk to an excited molecular state, as first proposed by Rous.[44] Here, it was observed that the significant enhancement (up to an order of magnitude) of the molecular cross section occurred if the energetic position of the molecular resonance coincided with the energetic position of an image state. An understanding of this process is hampered by the absence of realistic potentials to describe the image potential at the molecule−metal interface.

2.4. Relation of Decay Processes to Photoinduced Electron Transfer

Although the previous discussions have focused on ET from a metal surface to a molecular state/resonance, the reverse process, i.e., the decay of an excited molecular state/resonance via ET to the metal provides equally important information and is more accessible to experimental probes. We discuss two primary decay mechanisms with an emphasis on how they relate to photoinduced charge transfer: inelastic electron−electron scattering with bulk electrons and resonant charge transfer to bulk states (RET).

The inelastic electron−electron scattering rate is given by the following expression from many-body theory:[83]

$$\Gamma = -2 \int d\boldsymbol{r} \int d\boldsymbol{r}'\, \phi_i^*(\boldsymbol{r}) \mathrm{Im}[\sum(\boldsymbol{r},\boldsymbol{r}',\epsilon_i)] \phi_i(\boldsymbol{r}') \quad (18)$$

where ϕ_i and ϵ_i correspond the one particle eigenfunctions and eigenstates of the excited state; $\sum$ is the self-energy due to interaction of the electrons and can be computed from the screened Coulomb interaction in the so-called GW approximation; and Γ can be related to the lifetime through eq 4. This looks like a matrix element over the imaginary portion of the self-energy, except multiple integrations over space must occur to account for the nonlocality of the self-energy operator. The self-energy term incorporates the idea that the excited state can decay to the many unoccupied states that lie below it, such as unoccupied bulk metal states above the Fermi level. Despite its complexity, studies on image states have shown that the decay rate is dependent primarily on wave function overlap with the metal surface; this is similar to the wave function co-localization in determining the direct optical excitation rate.[83,84] Thus, by studying electron−electron decay processes at the interface, we can gain insight into wave function overlap between a molecular state/resonance and bulk states.

In contrast to inelastic decay via electron−electron scattering, RET occurs when localized states at the surface tunnel elastically into the bulk, i.e., the reverse process of hot-electron transfer. When one measures decay rates due to RET, then an estimate of the hot-electron transfer rate can be determined. Indeed, as pointed out by Gadzuk,[6] and by Harris and Holloway,[85] this leads to the following problem in resonance-assisted desorption: stronger coupling leads to stronger charge injection, but it also leads to reduced lifetimes, which reduces the amount of energy that can be transferred to nuclear coordinates and subsequently reduces the desorption or reaction probability.

Despite the abundance of indirect evidence for hot-electron transfer to molecular states/resonances, it is surprising that there has been little direct evidence for this channel in 2PPE experiments. Whether this is a result of a small cross section for the hot-electron attachment step or that for the ionization step remains an open question.

2.5. Electronic–Nuclear Coupling and Dynamic Localization

In all discussions presented previously, we focused our attention onto the electronic coordinates during photoinduced interfacial ET. Electronic−nuclear coupling, when necessary, can be treated as a perturbation. At this weak electronic−nuclear coupling limit, the electron is transferred mainly in an elastic and resonant process with a rate established by the overlap of the molecular wave function and substrate metal bands. The time scale of ET is given by the inverse of Γ discussed previously, as dictated by the Uncertainty Principle. This type of approach underlies coherent transport theories to describe ET through a metal−molecule−metal junction.[32,86] At the strong electronic−nuclear (and weak electronic-electronic) coupling limit, ET is controlled by nuclear rearrangement, as shown by Marcus and others in the so-called standard ET theory.[87] The rate of interfacial ET is determined by a thermal activation term, with the activation energy given by the nuclear reorganization energy (λ) and the free energy changes associated with the electron-transfer reaction.

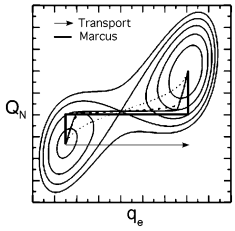

Figure 11. Hyper-potential energy surface (PES) for electron transfer (ET): q_e is the electron coordinate and Q_N is a nuclear (medium) coordinate. Adapted with permission from ref 94.

What is most difficult to describe from a theoretical perspective is the intermediate situation of interfacial electron-transfer accompanied by nuclear movement on the same time scale. This intermediate situation has been illustrated by recent time-resolved 2PPE experiments on small polaron formation[88] and electron solvation[89−92] in interfacial ET. An account by Petek and coworkers elsewhere in this issue provides a more detailed discussion on the subject.[93] The problem of solvation or small polaron formation during interfacial electron-transfer calls for the inclusion of both electronic and nuclear coordinates, such as the variational transition state theory applied by Truhlar and co-workers in treating charge-transfer reactions (see Figure 11).[94] In this representation, ET between two states is described by a trajectory on a two-dimensional hyper-potential energy surface (PES). Here, q_e represents the electron coordinate and Q_N a generic nuclear coordinate of the medium. In a coherent electron transport picture, such as Landauer type of theories, the electron transport process is represented by an arrow and nuclear coordinates are frozen. At the other extreme, the Marcus theory is represented by a thick solid line, where the rate-limiting nuclear fluctuation brings the two states into resonance, when tunneling and ET occurs. Reality is likely represented by the thin-solid, dashed, or dotted line (with increasing effective mass) where electronic and nuclear coordinates are not separable in the electron-transfer process.

We make three comments on the application of Figure 11 for interfacial ET:

(1) The two coordinates represent motions with drastically different masses;

(2) A real system may require more than two coordinates; and

(3) For interfacial ET between a metal and a molecule, the PES should be superimposed on an electronic continuum (the metal band structure).

3. The Two-Photon Photoemission Technique

Although several approaches have been used to probe photoinduced ET at surfaces, we focus on the two-photon

photoemission technique here. A 2PPE experiment can give information on the energetics, parallel dispersion, and lifetimes of excited interfacial states.[21,22,25−27] In a 2PPE experiment, the first photon (with energy typically lower than the surface work function, to avoid one-photon photoemission) is used to excite an electron into the intermediate state. A second photon ionizes this transient state, and the ejected electron is analyzed in energy, time, and momentum spaces. This simple description ignores the coherence between the pump and the probe process. To account for coherence, the Liouville von-Neuman equation must be solved. This has typically been conducted in a simplified three-level optical Bloch equation model with dephasing and relaxation accounted for parametrically.[95−98] More recent approaches have included the use of three coupled bands and also have accounted for interactions with phonons using modifications of the optical Bloch equations.[99,100]

In the simple case in which the intermediate state possesses no perpendicular dispersion, it is possible to distinguish an unoccupied from an occupied or a final state, based on how the kinetic energy of the photoemitted electron varies with photon energy. This is depicted in Figure 12 for the general case of bichromatic two-photon photoemission. The zero energy can be taken at the vacuum level so that E_u, E_i, and E_{Fermi} are negative; if the zero is taken at the Fermi level, then an offset (work function) must be added to yield an electron energy that is referenced to the Fermi level. The latter scale is labeled the final-state energy scale. Kinetic energy is useful when discussing angle-resolved measurements, because it is directly related to the parallel momentum vector, $k_{||}$, whereas binding energy relative to the vacuum level illustrates the energetics of image states and resonances the best. Because of the presence of both unoccupied states and occupied states in the 2PPE spectrum, the nature of peaks in the spectrum must be identified.

In addition to energetics, electron detectors with narrow angular resolution allow the measurement of dispersion, with respect to the parallel momentum vector. In the case of a surface with long-range order (i.e., surface band structure exists), crystal momentum parallel to the surface is conserved so that a simple relation holds between $k_{||}$, the angle of detection (θ) from the surface normal, and the kinetic energy, as given by

$$k_{||}(\text{Å}^{-1}) = \frac{\sqrt{2m_e E_{\text{kinetic}}}}{\hbar}\sin\theta = 0.511\sqrt{E_{\text{kinetic}}(\text{eV})}\sin\theta \quad (19)$$

In the majority of molecular systems, the electronic bandwidth is too small to show measurable dispersion. This is sometimes used to distinguish molecular states/resonances from image states/resonances at the surface: i.e., image states/resonances should give free-electron-like dispersions (with respect to $k_{||}$). However, exceptions to this are often found in the case of molecular electronic band formation and the localization of image states/resonances by interfacial potential fields due to the adsorbates.

A 2PPE experiment can be performed in the time domain by delaying the pump and probe pulses to determine (i) the rate of photoemission intensity decay, (ii) the time-dependent changes in electron energy, and (iii) the time-dependent change in parallel dispersions. The first type of experiment is a measure of population relaxation; this differs from energy width measurement, because lifetime broadening can result from population decay, dephasing, and heterogeneity. The second and third experiments probe the relaxation and localization dynamics, e.g., from an initially delocalized image state to a localized polaron.

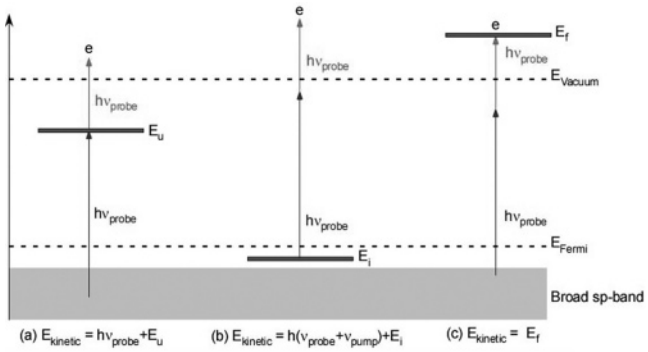

Figure 12. Schematic illustration of two-photon photoemission processes involving (a) an unoccupied intermediate state; (b) an occupied initial state; and (c) an unoccupied final state. Note the different dependences of electron kinetic energy on photon energies. The energies of the states are taken with respect to the vacuum level in this diagram.

Of significant importance to this article is the ability to control the polarization of the pump and probe laser pulses in a 2PPE experiment independently. This can be used to distinguish direct from indirect photoinduced ET in the first step. In the case of hot-electron transfer in the first step, the 2PPE signal is given by

$$W \propto \underbrace{(A_p \cos^2\theta + A_s \sin^2\theta)}_{\text{Pump Step}} \underbrace{|\vec{\mu}_{23}\cdot\mathbf{E}_{\text{probe}}|^2}_{\text{Probe Step}} \quad (20)$$

where A_p or A_s is the substrate absorbance for p- or s-polarized light at an incident angle θ; the last term is proportional to the ionization rate from the unoccupied state. By varying the polarization of the pump pulse, it is possible to determine if the observed signal follows the substrate absorbance. In the case of direct optical excitation in the first step, eq 10 must be multiplied by the ionization probability to give

$$W \propto (\sum_k |M_{k2}|^2 \delta(E_2 - E_k - \hbar\omega))|\vec{\mu}_{23}\cdot\mathbf{E}_{\text{probe}}|^2 \quad (21)$$

Note that this treatment neglects coherence between the pump and probe steps. If the initial states all have the same symmetry or there is only one initial state, a clear selection rule will be observed. However, if multiple initial states are involved in populating the transient state/resonance, the polarization dependence may not reflect a simple selection rule. In this case, the probe step should provide symmetry information of the transiently populated state or resonance, because the final state in photoemission should be totally symmetric in the case of normal emission.[58,101] This issue is well-established in angle-resolved UPS studies of molecular adsorbates, and we refer the reader to the excellent review by Steinrück.[58]

The actual implementation of time-, energy-, and angle-resolved two-photon photoemission is shown schematically for the setup in the authors' laboratory in Figure 13. Here, output from a femtosecond Ti:sapphire oscillator is frequency tripled or doubled into the ultraviolet (UV) region. The UV beam is subsequently split, in the case of monochromatic time-resolved 2PPE, into pump and probe paths with a pulse width of 80 fs. In the bichromatic 2PPE setup, the oscillator

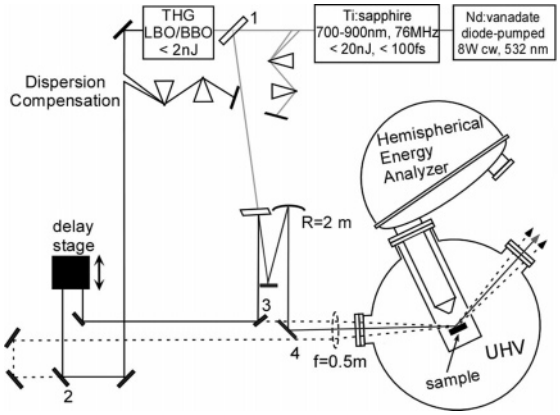

Figure 13. Schematic illustration of time-resolved 2PPE setup using an oscillator source and frequency tripling. The bichromatic setup is shown in the solid lines. After removal of the beam splitter (1) and mirrors (3 and 4), and the insertion of beam splitter into mirror mount (2) and addition of a focusing lens, it can then be used after realignment as a noncollinear monochromatic pump−probe setup. The dotted path shows the monochromatic beam paths. The sample can be cooled with liquid nitrogen (LN_2) to 90 K and resistively heated to >800 K.

output is split before the tripler or doubler to give an ultraviolet pump pulse and an infrared probe pulse. Here, the laser cavity can be tuned over a limited wavelength regime (~700−900 nm). For detection and determination of the electron kinetic energy, a hemispherical analyzer is used. Many variations of this system exist in multiple laboratories around the world. In particular, several notable improvements over the setup in Figure 13 include interferometry,[25] hemispherical detectors with one-dimensional (1D) arrays, widely tunable NOPA or OPA laser sources,[102] and more-sensitive time-of-flight (TOF) detectors. In addition, recent work has been performed using commercially available photoelectron emission microscopes, combined with two-photon photoemission, to allow spatial and temporal imaging of the sample.[103,104]

4. Examples

In this section, we present selected examples of 2PPE studies on photoinduced interfacial ET on metal surfaces. We group these results based on how they address the issues discussed earlier in section 2. We also attempt to identify limitations of current knowledge and ideas for future experiments.

4.1. The Role of Symmetry and the Projected Band Gap

The roles of adsorbate symmetry and projected band gaps on the direct photoinduced electron-transfer channel have been addressed in several model systems, including CO/Cu(111),[105,106] Cs/Cu,[64,107−112] and C_{60} on Cu(111) and Au(111).[113−115] In all examples, the unoccupied molecular or adsorbate states/resonances are believed to be populated by the direct-excitation mechanism.

The $2\pi^*$ resonance of CO on Cu(111) has been determined to have a lifetime of a few femtoseconds,[105,106] whereas the lifetime of the Cs antibonding resonance on Cu(111) is much longer (~50 fs at 33 K).[64] Initial work in the case of Cs/Cu(111) focused on the role of the projected band gap, because it limited RET to metal states with high $k_{||}$. This

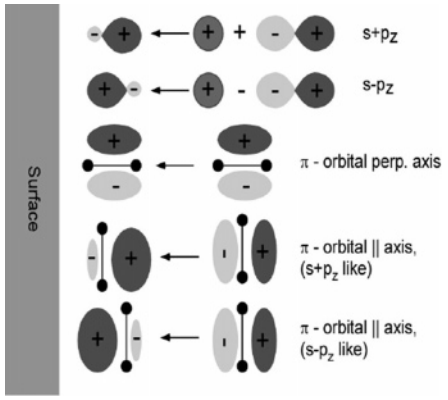

Figure 14. Qualitative illustration of how atomic or molecular orbitals hybridize at the surface due to the surface potential.

adequately explained the differences in lifetime observed on the different faces of copper.[109,110] However, this argument does not apply to the CO $2\pi^*$ resonance, which is also located in the projected band gap of Cu(111) but possesses an ultrashort lifetime. Instead, an explanation for difference between Cs and CO on the same Cu(111) surface requires an understanding of the symmetry: σ-symmetry for the antibonding Cs resonance and π-symmetry for the $2\pi^*$ CO resonance.

Consider the adsorption of an alkali atom on a metal surface. The image potential at the surface causes hybridization of the s and p orbitals. As illustrated in Figure 14, the $s-p_z$ orbital results in greater probability density near the surface and is involved in the bonding with the metal surface, whereas the $s + p_z$ orbital is more of antibonding character and has little electron density near the surface. The fact that the antibonding electron density is pushed away from the metal surface is a major reason for the long lifetime. In contrast to an atomic adsorbate, the interaction of a molecule is dependent on orientation. Consider the case of a molecular orbital with π-symmetry and nodal plane perpendicular to the surface. The π-orbital (or a π^*-orbital in the case of CO) is affected less by the image potential than one of σ-symmetry. Based on this argument, we expect the probability density of the $2\pi^*$ CO resonance to be closer to the metal surface than that of the σ^* Cs resonance, resulting in a shorter lifetime (faster ET rate) for the former. In contrast, if the nodal plane of the π-orbital is parallel to the surface plane, the probability density should be polarized similarly to the case of a σ orbital. A symmetry argument was also used to explain the LUMO resonance, which was absent in the case of pentafluorobenzene (C_6HF_5) but was observed in the cases of C_6F_6 and $C_6H_2F_4$,[116] although the mechanism is not clear.

The projected band gap is thought to be responsible for the different rates of photoinduced ET to the LUMO + 2 resonance of C_{60}, which is observed on Au(111), but not on Cu(111).[114,115] As shown in Figure 15, the LUMO + 2 level is an intense peak in 2PPE spectrum on Au(111), because of photoinduced ET from the metal surface; however, it is almost invisible on Cu(111). An examination of the energy-level diagram in Figure 16 provides a clue. The C_{60} LUMO + 2 level is resonant with the upper band on Au(111) but is located within the projected band gap on Cu(111). We expect stronger electronic coupling and, thus, a higher rate of direct photoinduced ET in the first excitation step in the former case.

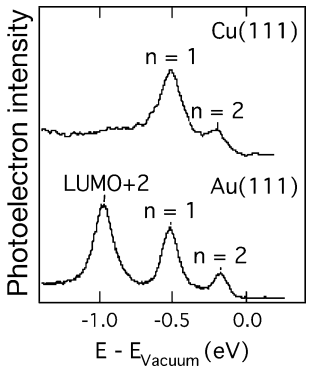

Figure 15. 2PPE spectra of 2ML of epitaxial C_{60} thin film on Cu(111) and Au(111). The $n = 1$ and 2 image resonances are shown, along with metal-to-LUMO+2 electron-transfer resonance on Au(111).[114,115]

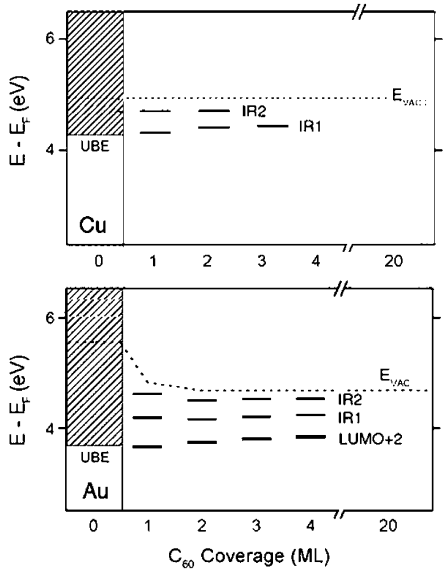

Figure 16. Energy-level diagram (referenced to the Fermi level) as a function of C_{60} film thickness on Cu(111) and Au(111). UBE denotes the upper band edge; IR1 and IR2 are image resonances.

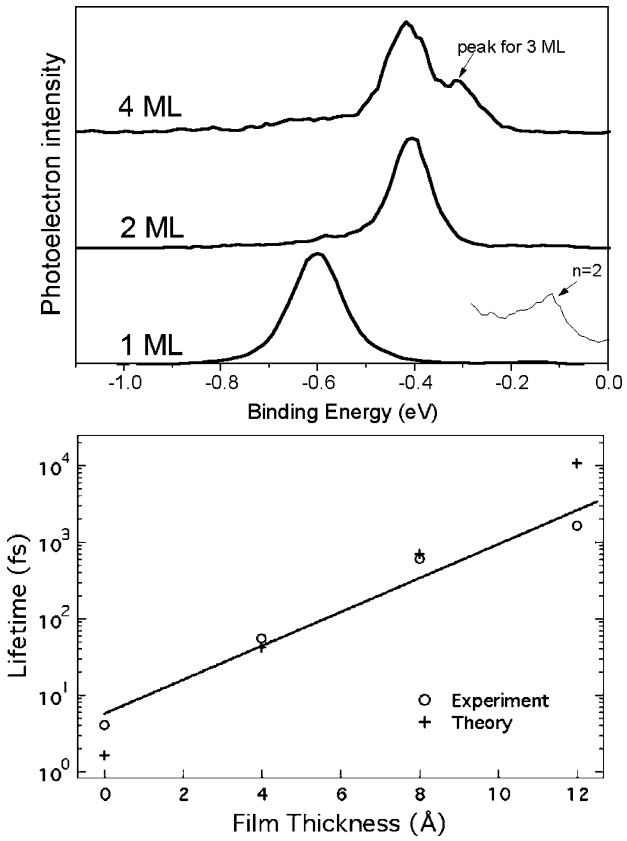

Figure 17. Left: 2PPE spectra for 1, 2, 4 ML *n*-heptane/Au(111). For coverage above 2 ML, island formation occurs and multiple peaks are observed, corresponding to patches of different film thicknesses. For a nominal coverage of 4 ML, only the bilayer and trilayer peaks are visible. A magnified view (10×) of the $n = 2$ image resonance for 1 ML is also shown. Right: Lifetime (τ) of the $n = 1$ image resonance as a function of the thickness (z) of the *n*-heptane film on Au(111). The circles are experimental data points and crosses are from an exact solution of the dielectric continuum model. The solid line is an exponential fit to experimental data: $\tau = \tau_o \exp(\beta z)$, with $\tau_o = 4$ fs and $\beta = 0.5$ Å^{-1}. Reprinted with permission from *J. Chem. Phys.*, ref 120. Copyright 2005, American Institute of Physics.

4.2. Molecular Film as an Insulator: Reduction in Resonant Electron Transfer Rates

Rare-gas atoms or molecules with large HOMO−LUMO gaps can serve as potential barriers for ET at the interface and may be used to control electron-transfer rates. Much work in this area has focused on rare-gas overlayers, because the simplicity of these systems allows for quantitative comparison between experiment and theory.[39,117,118] Harris and co-workers pioneered studies of the dynamics of image state electrons on alkane-covered metal surfaces.[43,119] As an example, Figure 17 shows results from our laboratory for the $n = 1$ image resonance on an *n*-heptane-covered Au(111) surface.[120] These results illustrate two important points: (i) the binding energy of the image resonance decreases as the film thickness increases, and (ii) the lifetime of the transiently populated image resonance increases (exponentially) as the film thickness increases. Both are due to the insulating nature of the molecular film, which pushes the image resonance wave function outside the adsorbate layer and further away from the metal surface. The decrease in image resonance binding energy is obvious when we consider Figure 3: the further the electron is from the surface, the weaker the image potential becomes (of course, polarization of the molecular film itself must also be taken into account). The exponential increase in lifetime can also be taken into account semi-quantitatively (see simulation results in Figure 17), by tunneling through the insulating layer, which is necessary for RET from the transiently populated image resonance to the metal substrate. In fact, these types of observations are signatures for image resonances on top of adsorbate films.

4.3. Chemisorption Bond and Interfacial Electron Transfer: Thiolate Self-Assembled Monolayers (SAMs)/Gold

Self-assembled monolayers (SAMs) of thiol molecules on metal surfaces have been popular model systems in research on electron transport.[121] This has motivated several 2PPE studies of the unoccupied electronic structure of these systems.[122−125] Vapor deposition of alkanethiol ($C_nH_{2n+1}SH$) on Au(111) in an ultravacuum environment can lead to the reclined (long molecular axis parallel to the surface) physisorbed alkanethiol phase, the reclined chemisorbed alkanethiolate ($C_nH_{2n+1}S$-) phase at low coverages, and the upright SAM phase at saturation coverage.[126] We have compared 2PPE spectra of these three phases for hexanethiol on Au(111) (see Figure 18). The formation of the Au−S bond

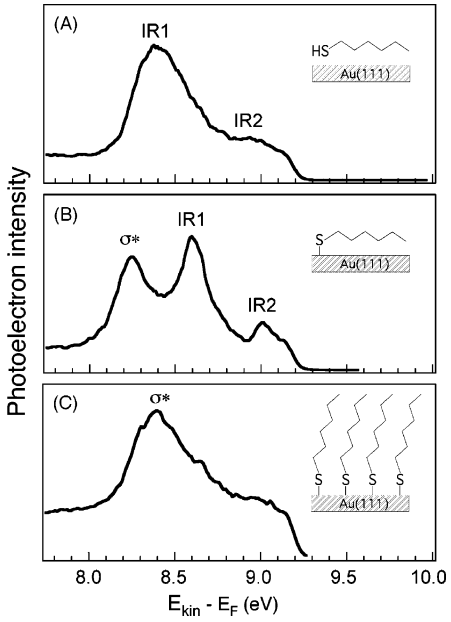

Figure 18. Monochromatic 2PPE spectra taken at $\hbar\nu = 4.59$ eV for (A) a physisorbed monolayer, (B) a chemisorbed reclined phase, and (C) a chemisorbed upright phase of *n*-hexane thiol on Au(111). The final state energy is referenced to the Fermi level.[125]

is evidenced by a localized σ^* resonance, which shows little parallel dispersion and broadens and shifts upward in energy when the reclined chemisorbed molecules become upright. For comparison, the image resonances (IR1 and IR2 for $n = 1$ and 2, respectively) show free-electron-like parallel dispersions. The lifetimes of image resonances on physisorbed or chemisorbed reclined phases are approximately the same; both are significantly shorter than those on monolayer *n*-heptane-covered gold. This suggests that the localized chemisorption bond does not affect the electronic coupling between delocalized image resonances and the metal substrate. Instead, lifetimes of image resonances are decreased due to scattering with S atoms within the thiol or thiolate monolayer. Interestingly, the S-metal σ^* resonance is observed at 3.7 eV (referenced to the Fermi level) on Au(111),[124] 3.3 eV on Cu(111),[122] and 1.6 eV on Ag(111).[123] It is not entirely clear why the σ^* resonance on Ag(111) is substantially lower in energy than that on Au(111) or Cu(111). One explanation is the involvement of the d-band in S-metal bonding. The d-band is located at ~2 eV below the Fermi level on Au or Cu, but ~4 eV below the Fermi level on Ag. Perebeinos and Newton[127] recently performed DFT calculations and suggested an alternative explanation for the observed resonance; they attributed it to the S−C antibonding orbital in benzenethiolate on gold, but this seems to be inconsistent with the observation in Figure 18, that the resonance is only observed when adsorbed thiols dissociate to thiolates.

In addition to the localized σ^* and delocalized image resonances, Zhu and co-workers also observed an image-like delocalized resonance in the upright SAM phases of alkanthiolates.[125] This resonance in not clearly resolved in the monochromatic 2PPE spectrum (C) in Figure 18, but does become well-resolved in bichromatic measurements (see Figure 19). This peak is labeled "IFR" for interfacial resonance. Angle-resolved measurements show that the IFR possesses free-electron-like parallel dispersion (upper panel in Figure 19), with an effective electron mass of ~1 m_e.

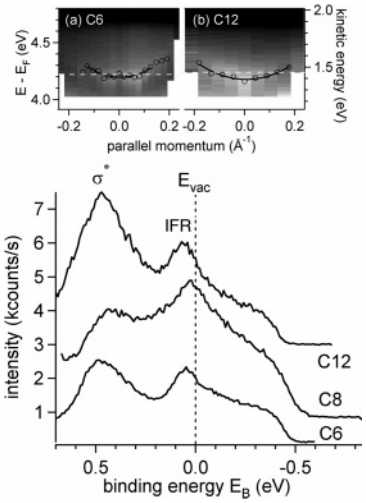

Figure 19. Bichromatic 2PPE spectra ($\hbar\nu_1 = 4.65$ eV, $\hbar\nu_2 = 1.55$ eV) of alkanethiolate SAMs on Au(111). The energy scale is the binding energy of the intermediate state. The spectra are vertically offset for better visibility. The upper inset shows 2PPE dispersion maps of (a) hexane thiolate and (b) dodecane thiolate SAMs on Au(111). The 2PPE intensity is plotted as a function of parallel momentum and intermediate state energy on a linear grayscale.[125]

The short lifetime (<30 fs) and the insensitivity of the energy level (binding energy of BE = 0.045 ± 0.010 eV) to molecular length (and, thus, layer thickness) suggest that the probability density of the electron wave function is concentrated inside the molecular layer close to the SAM/gold interface. For comparison, the properties of a conventional image resonance on top of a saturated hydrocarbon film is a strong function of film thickness (see Figure 17). The interfacial resonance results from the image-like potential at the SAM/Au interface. The presence of image-like resonances at adsorbate−metal interfaces was first reported by Höfer and co-workers for the Ar/Cu(100) system.[128]

4.4 Band-to-Band Interfacial Electron Transfer

When the adsorbate layer is ordered on the metal surface and there is significant intermolecular interaction, conduction bands can form from unoccupied molecular orbitals. This leads to the possibility of photoinduced band-to-band ET between the metal substrate and the molecular layer. This scenario has been discovered recently in the model system of epitaxial thin films of C_{60} on Au(111).[129] As shown in Figure 15, the C_{60} LUMO + 2 resonance can be populated by direct photoinduced ET from the Au substrate.[118] The band nature of the molecular resonance is established by dispersion in the surface plane. Figure 20 shows parallel dispersions of the molecular resonance for 1 and 2 monolayer (ML) C_{60}/Au(111) obtained from angle-resolved measurement conducted in a plane that contained the surface normal (111) and the parallel momentum direction, as defined in Figure 20. Because of the large unit cell size of the C_{60} superlattice, the dispersion measurements cover $k_{||}$ values beyond the first Brillioun zone. These dispersions can be well-described by calculated bands (solid and dashed curves) from tight binding theory of S-symmetry. The approximation of S symmetry is justified by the fact that the molecular dispersions have almost the same shapes as those of the image resonances that are known to possess S symmetry. The molecular band evolves into a quantum well with increasing number of C_{60} overlayers, as characterized by band

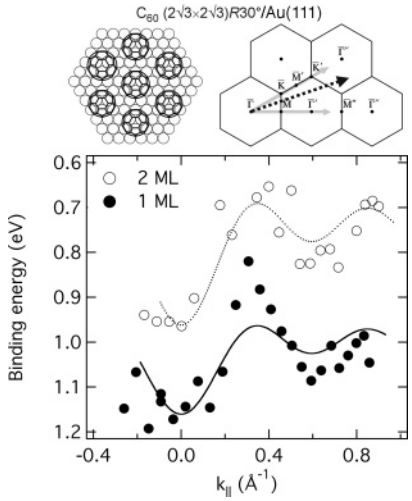

Figure 20. Parallel dispersions of the LUMO+2 molecular resonance on 1 ML (solid circles) and 2 ML (open circles) C_{60}-covered Au(111). The solid and dashed curved are fits to the tight binding approximation, which gives an intermolecular charge-transfer integral of $\beta = -0.033 \pm 0.003$ eV. The schematics at the top of the figure illustrate the C_{60} $(2\sqrt{3} \times 2\sqrt{3})$R30° superlattice on Au(111) and the Brillouin zones of the C_{60} superlattice. The dashed arrow indicates the $k_{||}$ direction for dispersion measurements.[129]

splitting (data not shown). Time-resolved 2PPE measurements reveal that the lifetimes of the molecular quantum well are below the detection limit of the laser pulse duration (100 fs). This puts an upper limit of ~20 fs on the lifetime of the transiently populated resonance. A lower limit of the lifetime of 4 fs is obtained from the width of the molecular resonance.

4.5. Evidence of Hot-Electron Transfer in 2PPE

Although indirect evidence for photoinduced hot-electron transfer is abundant, particularly from surface photochemical studies on metal and semiconductor surfaces,[4−9] direct evidence for the presence of the transient anion is rare. Polarization-dependent 2PPE measurements, as described in eqs 20 and 21, have suggested that a σ state in the CO/Cu(111) system was populated by hot-electron transfer.[96] Recent work of Lee et al. on phenol on Ag(111) correlated surface photochemistry with 2PPE measurement.[130] The photochemical cross section was determined to be dependent exponentially on photon energy, which is consistent with hot-electron transfer to an adsorbate resonance energetically located at ~3.2−3.5 eV above the Fermi level.[131,132] Indeed, two-photon photoemission measurements reveal a nondispersive state located at 3.22 eV above the Fermi level on the phenol-covered Ag(111) surface.[130] Supporting this assignment, polarization measurements with p- and s-polarized pump light show that the photoemission intensity scales with the substrate absorbance. The combination of these observations provides evidence that the observed resonance is due to hot-electron transfer, not direct optical excitation. Similarly, Ryu et al. showed that the intensity ratio of the $n = 1$ image state on Ag(111) under the irradiation of p- and s- polarized pump lasers is consistent with the substrate absorbance, in accordance with hot-electron transfer to the image state.[82] This is different from measurements on other surfaces, e.g., Cu(111), where the image states cannot be excited with s-polarized pump light.[96] The reason for the different behaviors is not understood and deserves further clarification.

4.6. Interfacial Electron Transfer Rates

As previously discussed, lifetime measurements provide quantitative information on the electron-transfer coupling term, $\hat{V}_{ET}$. Here, we focus on two examples in which the lifetimes of the molecular resonances have been determined. The first example is C_{60} thin films epitaxially grown on the (111) face of noble metals;[113−115,132−135] the initial optical excitation is mainly intramolecular in nature and forms excitons whose quenching rates vary as a function of film thickness in a manner that is not consistent with the traditional tunneling picture. Unlike the excitons, the lifetime of the LUMO + 2 quantum well transiently populated by direct metal-to-molecule photoinduced ET (see section 4.4) is much shorter and it is below the detection limit of the laser pulses that have been used. The second example is C_6F_6 thin films adsorbed on noble-metal surfaces. Here, the initial excitation is direct photoinduced ET from the metal substrate to the LUMO state to form a transient anion with a measurable lifetime. This molecular state is energetically outside the region of image states or resonances on these surfaces.[76,116,136] There is a fundamental difference between the two examples: the former is a charge-neutral excited state that involves a photogenerated hole on the C_{60} molecule, whereas the latter involves a transient molecular anion. Note that the ET rate measured by 2PPE is different than that from the core−hole clock method,[137−142] which is not discussed here.

4.6.1. Electron Transfer between C_{60} Excitons and Noble-Metal Surfaces

Our group has conducted 2PPE studies of epitaxial C_{60} films on Cu(111) and Au(111).[113−115] There was a misassignment of energy levels in the first publication[113] that was corrected later.[114] We illustrate the results on C_{60}/Au here.

Figure 21 shows a set of monochromatic 2PPE spectra taken at different photon energies for 2 ML C_{60}/Au(111). This system provides perhaps the richest information among 2PPE studies on metal−molecule interfaces. The dependences of peak positions on photon energy reveal the occupied, unoccupied, and final state origins of the photoelectron (see Figure 12). Here, peak H corresponds to two-photon ionization of the HOMO; L2 is photoinduced ET from the substrate to the LUMO + 2 level. L1* and L2* correspond to Frenkel excitons (intramolecular) involving the LUMO + 1 and LUMO + 2 levels, respectively. The peaks labeled F0*−F3* are excitons with the excited electron above the vacuum level. Peaks IR1 and IR2 are photoinduced direct ET to image resonances. Note that the exciton that corresponds to the LUMO level was not accessed, because the probe photon energy was not large enough. With increasing thickness, the spectral features due to metal-to-molecule ET decreases and become negligible for film thicknesses of >7 ML. However, all peaks due to excitons and photoionization of the HOMO persist for thicker films. The energy levels mapped out by 2PPE are summarized in Figure 22. Similar results were obtained for the epitaxial C_{60}/Cu(111) interface, except that the LUMO + 2 level was not observed (see Figures 15 and 16).

We now focus on the distance-dependent decay dynamics of the exciton that involves the LUMO + 1 level. Here, the

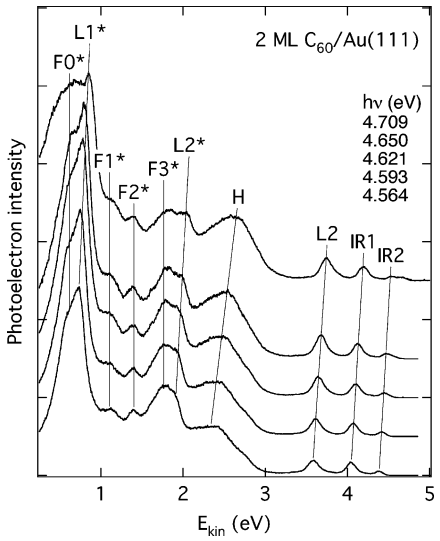

Figure 21. 2PPE spectra of 2 ML C_{60}/Au(111) taken at the indicated photon energies ($\hbar\nu = 4.563-4.709$ eV). Each spectrum is shifted upward vertically by an amount proportional to the photon energy. The solid lines labeled L1*, L2*, L1, L2, IR1, and IR2 correspond to one-photon dependences of the peak position; those labeled F0*, F1*, F2*, and F3* are independent of photon energy; the line labeled H corresponds to the two-photon dependence of peak position. The *x*-axis is the kinetic energy of the photoelectron referenced to the vacuum level. Reprinted with permission from *Phys. Rev. B* (http://link.aps.org/abstract/PRB/v72/p045441), ref 115. Copyright 2005 American Physical Society.

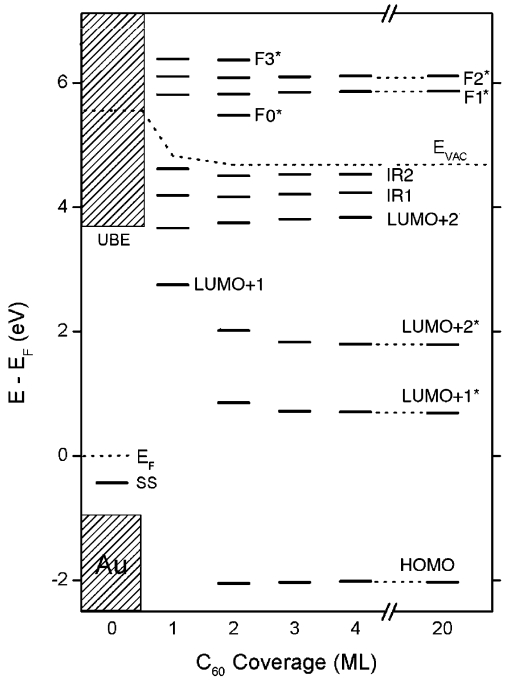

Figure 22. Energy-level diagram of the C_{60} epitaxial film on Au(111), as measured by 2PPE. The peaks labeled LUMO+1 and LUMO+2 are due to metal-to-molecule electron transfer (ET). The peaks labeled LUMO+1* and LUMO+2* are corresponding levels involved in Frenkel excitons. E_F is the Fermi level, and E_{vac} is the vacuum level. Also shown in the projected band gap of Au in the (111) direction. After Dutton et al.[115] Results on Cu(111) are similar, except that the LUMO+2 level is almost invisible (see Figure 14). Reproduced with permission from *Phys. Rev. B* (http://link.aps.org/abstract/PRB/v72/p045441), ref 115. Copyright 2005 American Physical Society.

lifetime of the exciton is followed in a pump−probe cross-correlation experiment. Figure 23 shows the measured

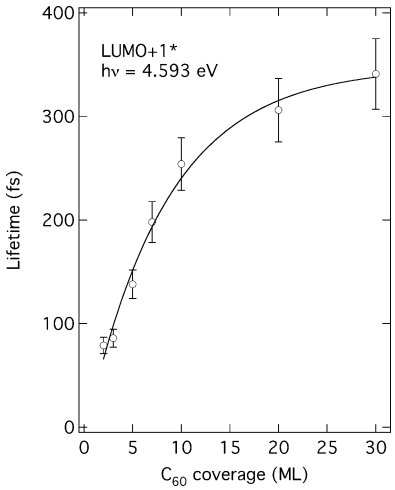

Figure 23. Lifetimes (circles) of the LUMO+1* exciton state, as a function of the C_{60} thickness on Au(111). The solid line is fit to an exponential function with an asymptotic lifetime value of $\tau = 345 \pm 10$ fs. Reproduced with permission from *Phys. Rev. B* (http://link.aps.org/abstract/PRB/v72/p045441), ref 115. Copyright 2005 American Physical Society.

lifetimes as a function of film thickness. The solid curve is an exponential fit which yields an asymptotic value of 345 ± 10 fs. This asymptotic value corresponds to the intrinsic lifetime of the exciton in solid C_{60}, which is likely due to decay from the LUMO + 1 level to the LUMO level. Note that the photoemission signal is dominated from the top-most C_{60} layer, because of the small electron escape depth.[115] The decrease of the lifetime as distance to the metal surface shortens is due to quenching by the gold substrate. The most efficient quenching mechanism is likely RET from the transiently populated LUMO + 1 level in C_{60} to unoccupied states in gold and the filling of the transient hole in C_{60} by a metal electron. At each coverage, the decay rate ($1/\tau$) is the sum of two contributions: the decay rate intrinsic to the C_{60} film at this exciton energy ($1/\tau_a$, $\tau_a = 345$ fs) and an external rate (k_q, s^{-1}) that is due to RET to the metal substrate. The resulting quenching rates (solid circles) are shown as a function of distance to the gold surface in a semilogarithmic plot in Figure 24. In a simple picture that depicts tunneling through a barrier, the RET rate is expected to be dependent exponentially on distance (d),

$$k_{RET} = k_o \exp(-\beta d)$$

where the characteristic distance parameter β typically lies in the range of 0.9−1.3 $Å^{-1}$ for saturated alkanes and as small as 0.2 $Å^{-1}$ for some π-conjugated molecules.[144] The solid line in Figure 24 is fit to this exponential relationship, yielding $\beta = 0.023 \pm 0.05$ $Å^{-1}$ and $k_o = 1.2 \times 10^{13}$ s^{-1}, which corresponds to an interfacial electronic coupling strength or spectral density of $\Gamma_o = 8$ meV. This can be compared to earlier measurements of the LUMO + 1* exciton lifetime, as a function of the distance of C_{60} to the Cu(111) surface (performed at a different wavelength).[114] In this system, the β value was determined to be 0.11 $Å^{-1}$ and $\Gamma_0 \approx 60$ meV. The stronger coupling observed on Cu(111) is not surprising, because it is known that the interaction between C_{60} and the metal surface is much stronger on Cu(111) than on Au(111). Upon adsorption, there is a transfer of 1.5−2 electrons to each C_{60} molecule from the Cu surface[145,146] versus little to no static charge transfer that occurs on the Au(111) surface.[147]

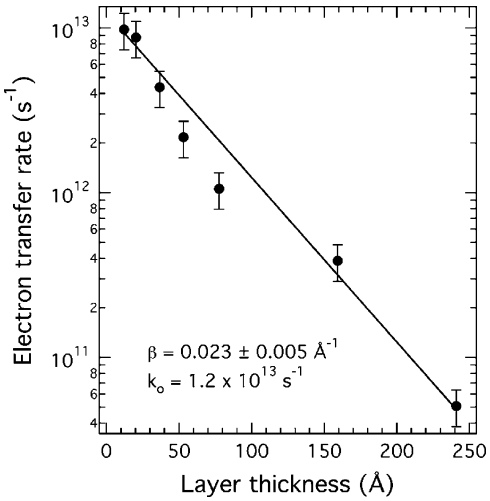

Figure 24. Semilogarithmic plot of quenching rate (by the metal substrate) of the LUMO+1* exciton, as a function of the C_{60} overlayer thickness. Solid line is the fit to an exponential function that gives the indicated parameters. Reproduced with permission from *Phys. Rev. B* (http://link.aps.org/abstract/PRB/v72/p045441), ref 115. Copyright 2005 American Physical Society.

The β value obtained for ET from the LUMO + 1* exciton of C_{60} to the metal surface is much smaller than those typical values for tunneling. It is inadequate to consider such a weak distance dependence as tunneling. Electronic excitons in solid C_{60} are known to form an effective band, with estimated bandwidth as high as 10^2 meV from theory. The interfacial electronic coupling strength (spectral density) between LUMO + 1* and the metal substrate is smaller than the estimated electronic exciton bandwidth. With increasing C_{60} thickness, $|\Psi|^2$ within a delocalized C_{60} exciton band is further away from the interface; as a result, its coupling to the gold substrate decreases and the ET rate decreases.

4.6.2. The Transient Anionic State in C_6F_6 on Noble-Metal Surfaces

The C_6F_6/Cu(111)[76,116,136,143] or C_6F_6/Au(111)[148] system possesses a ET state that involves direct photoexcitation from the metal to the LUMO of C_6F_6. Consequently, this is a transiently populated anionic state. This has been substantiated by the agreement between the energetic position found in inverse photoemission[149] and the 2PPE measurements.[76,116,136,143] The anionic state has been assigned to the σ^* C−F orbitals.[136,143] The initial photoexcitation is direct and is subsequently a result of the $\hat{V}_{PMS}$ term in eq 3. Evidence for this can be seen in Figure 25, which shows the polarization dependence for C_6F_6 on Au(111); the molecular state can only be excited with p-polarized light, not with s-polarization.[148] The anionic molecular state is located at ~3 eV (above the Fermi level) on Cu(111) and ~3.5 eV on Au(111). Parallel dispersions show almost free-electron-like behavior. In the case of C_6F_6/Cu(111), the effective electron mass decreases from 2 m_e at 1 ML to 1 m_e at 5 ML C_6F_6 coverage, whereas the lifetime increases from ≤10 fs to ~30 fs in the same coverage range.

The latest results from the Wolf group are shown in Figure 26 for 2PPE spectra from C_6F_6/Cu(111), as a function of layer thickness.[76] There are two peaks for the anionic resonance: peak A, which decreases in energetic position with increasing coverage, and peak B, whose position is fixed in energy. Here, peak A is assigned to the LUMO, whereas peak B has been speculated to be due to excimers; however,

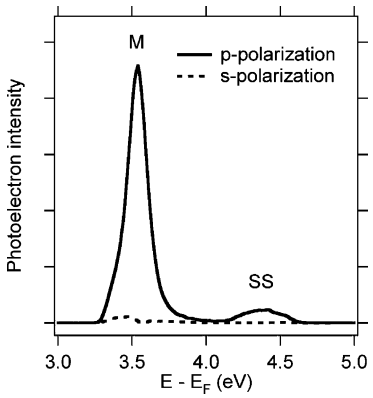

Figure 25. Polarization-dependent 2PPE spectra for C_6F_6/Au(111) at 1 ML coverage. The probe photon energy is 1.55 eV, and the pump photon energy is 4.65 eV. Peak M is the molecular anionic state, and SS is the Au(111) surface state.[148]

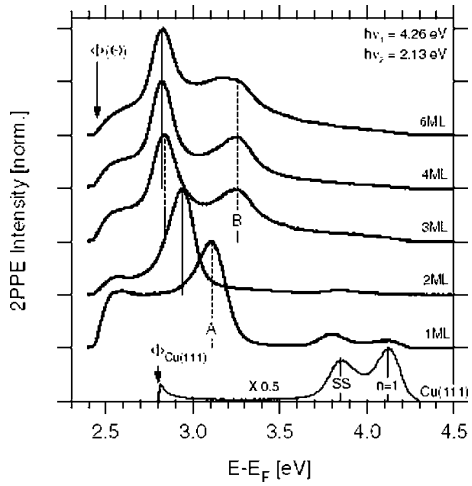

Figure 26. Bichromatic 2PPE spectra recorded for various coverages of C_6F_6 on Cu(111) at zero time delay from bare Cu(111) (bottom) to 6 ML C_6F_6/Cu(111) (top) normalized to peak intensity. Reproduced with permission from *New J. Phys.*, ref 76. Copyright 2005 IOP Publishing Limited.

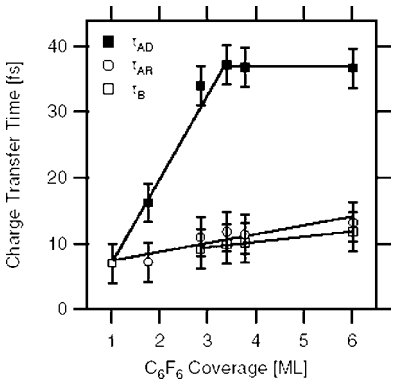

Figure 27. C_6F_6 coverage dependence on Cu(111) of extracted decay times τ_{AD} (■) and τ_B (□) for states A and B and rise time τ_{AR} (○) for state A. τ_{AD} increases up to $\Theta = 3$ ML and stays constant for higher coverages. In contrast, τ_{AR} and τ_B exhibit only a weak monotonic increase with coverage. The solid lines are in place to guide the eye. Reproduced with permission from *New J. Phys.*, ref 76. Copyright 2005, IOP Publishing Limited.

no conclusive assignment has been given. The lifetime of peak A saturates after the coverage increases to 3ML as shown in Figure 27; at 1 ML, a lifetime of 7 fs corresponds to an interfacial coupling strength of 95 meV. Interestingly, pump−probe cross-correlation measurement reveals that

there is a finite rise time associated with peak A. Initially, this rise time was thought to occur due to interband decay from peak B; however, this has now been shown to not be the case. The combination of time- and angle-resolved measurements in this system showed a $k_{||}$-dependent decay rate for peak A. The authors suggest that intraband decay is responsible for the rise time that has been observed in prior experiments.

There are several puzzles associated with the C_6F_6 systems. It is not known why the anionic resonance forms a free-electron-like delocalized electronic band and how this adsorbate band effectively couples to the metal electronic band. We also do not understand the role of the image potential on the formation of this LUMO band. Theoretical treatment of this problem is difficult, because one must effectively couple the molecular potential with the image potential, which is a difficult task at the present time.

4.7. Dynamic Localization: Solvation and Polaron Formation

One of the most fascinating problems in photoinduced interfacial ET is the role of electronic−nuclear coupling and dynamic localization. One of us argued earlier that surface photochemistry could be viewed as one consequence of dynamic localization.[21] Time-resolved 2PPE has allowed a direct view of the electron localization dynamics in time, energy, and momentum spaces. This issue has been reviewed recently by Harris and co-workers[150] and Bovensiepen,[151] as well as by Petek and coworkers in this issue of *Chemical Review*.[93] Successful examples include small polaron formation from image states on alkane-covered Ag(111);[88] solvation of an image-state electron in acetonenitrile, butyronitrile, and alcohol thin films on Ag(111);[91,152] electron solvation in amorphous or crystalline ice thin films on Cu(111) or Ru(001);[89,90,153] and electron solvation in water or methanol thin films on TiO_2.[92] The readers are referred to more-detailed accounts of these examples in the aforementioned reviews. In the following, we illustrate dynamic localization in photoinduced interfacial ET using an example from our laboratory: localization of an image state in nonane thin films on Cu(111).[148]

Figure 28 shows a two-dimensional map representation of 2PPE spectra, as a function of pump−probe delay for the $n = 1$ image state on ~1.5 ML nonane/Cu(111). At this coverage, the surface consists of domains of 1 and 2 ML nonane islands. As expected, the binding energy of the $n = 1$ image state decreases from the clean surface value of 0.82 eV to 0.49 eV on 1 ML nonane-covered surfaces and 0.38 eV on 2 ML nonane-covered surfaces. Although the lifetime of the $n = 1$ image resonance on 1 ML covered surface is too short to allow for the observation of energy relaxation, it is clearly observed on the 2 ML nonane-covered surface. For the $n = 1$ image state on 2 ML nonane/Cu(111), the electron energy decreases by 40 meV for times of ≥1 ps, with a single-exponential relaxation lifetime of $\tau = 0.5$ ps. This energy relaxation is accompanied by the disappearance in parallel dispersion, with an effective electron mass increasing from ~1 m_e at zero time delay to >10 m_e at a time delay of 1 ps.

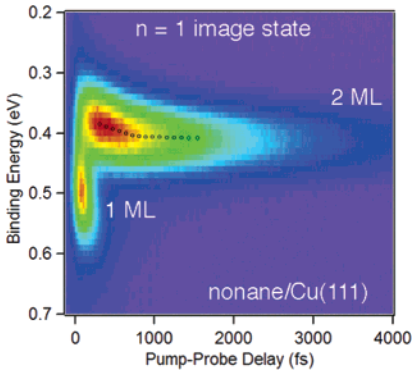

Figure 28. Two-dimensional (2D) representation of 2PPE spectra, as a function of pump−probe delay for the $n = 1$ image state on ~1.5 ML nonane/Cu(111). The false color represents the intensity of 2PPE spectra. Note that, at this coverage, the surface consists of domains of 1 and 2 ML nonane islands.

The aforementioned observations on the localization of an image state in both energy and momentum ($k_{||}$) spaces are in qualitative agreement with results from the pioneering of Harris and co-workers, who attributed the dynamic localization to the self-trapping of a small polaron, which is a result of the dynamic deformation of the two-dimensional alkane lattice, because of the transient presence of an excited electron. Interestingly, the amount of electron energy stabilization (~40 meV) observed in Figure 28 for 2 ML nonane/Cu(111) is significantly larger than the value of ≤10 meV that has been observed for alkane/Ag(111).[88] We suggest that the details of the adsorbate film structure and morphology are important to dynamic localization, and defects or disorder within the two-dimensional adsorbate structure may determine the extent of energy relaxation. This suggestion correlates well with recent observations on the dramatic difference in electron solvation dynamics between amorphous ice and crystalline ice thin films. For amorphous-ice thin films on Ru(001), electron solvation and dynamic localization leads to an energy stabilization of ~300 meV within 0.5 ps,[153] and for crystalline ice thin films on Ru(001), there is no observable energy stabilization for the solvated electron within 1 ps. Instead, much longer time scales (seconds to minutes) are needed to observe electron energy relaxation.[154]

5. Concluding Remarks

Photoinduced ET at molecule−metal and molecule−semiconductor interfaces is a common problem underlying many important chemical and physical processes, such as solar energy conversion, molecular optoelectronics, and photocatalysis. This account summarizes our current understanding from (or the limitation of) time-, energy-, and momentum-resolved two-photon photoemission experiments. A particularly important and unique discovery from these experiments is the dominance of a direct, photoinduced metal-to-molecule electron-transfer channel. We suggest that such a direct mechanism should also be important in other processes, such as dye-sensitized solar energy conversion or nanoscopic molecular optoelectronic devices. We discuss the importance of interfacial electronic coupling and wave function mixing in determining the direct channel of metal-to-molecule ET, the indirect channel of hot-electron transfer, and the reverse processes of molecule-to-metal ET. Symmetry of the molecular orbital and the local adsorption site, as well as the projected metal band structure, can serve as simple criteria in determining whether the direct channel is operative; however, a quantitative assessment of the optical transition probability remains a major challenge. An exciting development in time-resolved two-photon photoemission studies of adsorbate−metal interfaces is the probe of electronic−nuclear coupling and dynamic localization. These

experiments are bridging the traditional views on coherent electron transport and incoherent ET at metal−molecule interfaces.

6. Acknowledgment

We thank the National Science Foundation, through Grant DMR 02383307 and the MRSEC Program under Award Number DMR 0212302, and the Department of Energy, through Grant DE-FG02-05ER46252 A001, for financial support. C.D.L. thanks the University of Minnesota for support of a Doctoral Dissertation Fellowship during this work.

7. References

(1) Kamat, P. V. *Chem. Rev.* **1993**, *93*, 267.
(2) Bard, A. J.; Fox, M. A. *Acc. Chem. Res.* **1995**, *28*, 141.
(3) Linsebigler, A. L.; Lu, G.; Yates, J. T., Jr. *Chem. Rev.* **1995**, *95*, 735.
(4) Avouris, Ph.; Walkup, R. E. *Annu. Rev. Phys. Chem.* **1989**, *40*, 173.
(5) Zhou, X. L.; Zhu, X.-Y.; White, J. M. *Surf. Sci. Rep.* **1991**, *13*, 73.
(6) Gadzuk, J. W. *Surf. Sci.* **1995**, *342*, 345.
(7) Guo, H.; Saalfrank, P.; Seidemann, T. *Prog. Surf. Sci.* **1999**, *62*, 239.
(8) Zimmermann, F. M.; Ho, W. *Surf. Sci. Rep.* **1995**, *22*, 127.
(9) Zhu, X.-Y. *Annu. Rev. Phys. Chem.* **1994**, *45*, 113.
(10) Hagfeld, A.; Gratzel, M. *Chem. Rev.* **1995**, *95*, 49.
(11) Hagfeld, A.; Gratzel, M. *Acct. Chem. Res.* **2000**, *33*, 269.
(12) Gratzel, M. *MRS Bull.* **2005**, *30* (1), 23.
(13) Gregg, B. A. *MRS Bull.* **2005**, *30* (1), 20.
(14) Forrest, S. R. *MRS Bull.* **2005**, *30* (1), 28.
(15) Galperin, M.; Nitzan, A. *Phys. Rev. Lett.* **2005**, *95*, 206802.
(16) Newns, D. M. *Phys. Rev.* **1969**, *178*, 1123.
(17) Anderson, N. A.; Lian, T. *Annu. Rev. Phys. Chem.* **2005**, *56*, 491.
(18) Chance, R. R.; Prock, A.; Silbey, R. *Adv. Chem. Phys.* **1978**, *37*, 1.
(19) Whitmore, P. M.; Robota, P. M.; Harris, C. B. *J. Chem. Phys.* **1982**, *76*, 740.
(20) Whitmore, P. M.; Alivisatos, A. P.; Harris, C. B. *Phys. Rev. Lett.* **1983**, *50*, 1092.
(21) Zhu, X.-Y. *Annu. Rev. Phys. Chem.* **2002**, *53*, 221.
(22) Zhu, X.-Y. *Surf. Sci. Rep.* **2004**, *56*, 1.
(23) Calvert, J. G.; Pitts, J. N., Jr. *Photochemistry*; Wiley: New York, 1966.
(24) Hufner, S. *Photoelectron Spectroscopy: Principles and Applications*, 3rd Edition; Springer−Verlag: Berlin, 2003.
(25) Petek, H.; Ogawa, S. *Prog. Surf. Sci.* **1997**, *56*, 239.
(26) Weinelt, M. *J. Phys.: Condens. Matter* **2002**, *14*, R1099.
(27) Fauster, Th.; Steinmann, W. In *Photonic Probes of Surfaces, Electromagnetic Waves: Recent Developments in Research*; Halevi P., Ed.; North−Holland: Amsterdam, 1995.
(28) Norskov, J. K. *Rep. Prog. Phys.* **1990**, *53*, 1253.
(29) Scheffler, M.; Stampfl, C. In *Handbook of Surface Science, Vol. 2: Electronic Structure*; Horn, K., Scheffler, M., Eds.; Elsevier: Amsterdam, 2000.
(30) Gross, A. *Theoretical Surface Science: A Microscopic Perspective*; Springer−Verlag: Berlin, 2003.
(31) Brivio, G. P.; Trioni, M. I. *Rev. Mod. Phys.* **1999**, *71*, 232.
(32) Nitzan, A. *Annu. Rev. Phys. Chem.* **2001**, *52*, 681.
(33) Nakamura H.; Yamashita, K. *J. Chem. Phys.* **2005**, *122*, 194706.
(34) Zangwill, A. *Physics at Surfaces*; Cambridge University Press: Cambridge, U.K., 1988.
(35) Shockley, W. *Phys. Rev.* **1939**, *56*, 317.
(36) Echenique, P. M.; Pendry, J. B. *J. Phys. C* **1978**, *11*, 2065.
(37) Echenique, P. M.; Pendry, J. B. *Prog. Surf. Sci.* **1990**, *32*, 111.
(38) Echenique, P. M.; Pitarke, J. M.; Chulkov, E. V.; Silkin, V. M. *J. Electron Spectrosc. Relat. Phenom.* **2002**, *126*, 165.
(39) Echenique, P. M.; Berndt, R.; Chulkov, E. V.; Fauster, Th.; Goldmann, A.; Höfer, U. *Surf. Sci. Rep.* **2004**, *52*, 219.
(40) Chulkov, E. V.; Silkin, V. M.; Echenique, P. M. *Surf. Sci.* **1999**, *437*, 330.
(41) Chulkov, E. V.; Silkin, V. M.; Echenique, P. M. *Surf. Sci.* **1997**, *391*, L1217.
(42) Osgood, R. M., Jr.; Wang, X. *Solid State Phys.* **1998**, *51*, 1.
(43) Harris, C. B.; Ge, N.-H.; Lingle, R. L., Jr.; McNeill, J. D.; Wong, C. M. *Annu. Rev. Phys. Chem.* **1997**, *48*, 711.
(44) Rous, P. J. *Phys. Rev. Lett.* **1995**, *74*, 1835.
(45) Gao, S.; Langreth, D. C. *Surf. Sci. Lett.* **1998**, *398*, L314.
(46) Nagesha, K.; Sanche, L. *Phys. Rev. Lett.* **1998**, *81*, 5892.
(47) Frank, K.-H.; Dudde, R.; Koch, E. E. *Chem. Phys. Lett.* **1986**, *132*, 83.
(48) Frank, K. H.; Yannoulis, P.; Dudde, R.; Koch, E. E. *J. Chem. Phys.* **1988**, *89*, 7569.
(49) Marinica, D. C.; Ramseyer, C.; Borisov, A. G.; Teillet-Billy, D.; Gauyacq, J. P. *Surf. Sci.* **2003**, *540*, 457.
(50) Mukamel, S. *Principles of Nonlinear Optical Spectroscopy*; Oxford University Press: New York, 1995; p 36.
(51) Weisskopf, V. F.; Wigner, E. P. *Z. Phys.* **1930**, *63*, 54.
(52) Deleted in proof.
(53) Boyd, R. W. *Nonlinear Optics*, 2nd Edition; Academic Press: New York, 2003.
(54) Levinson, H. J.; Plummer, E. W.; Feibelman, P. J. *Phys. Rev. Lett.* **1979**, *43*, 952.
(55) Feibelman, P. J. *Prog. Surf. Sci.* **1979**, *12*, 287.
(56) Boukaert, L. P.; Smoluchowski, R.; Wigner, E. *Phys. Rev.* **1936**, *50*, 58.
(57) Lax, M. *Symmetry Principles in Solid State and Molecular Physics*; Dover Publications: Mineola, NY, 2001.
(58) Steinruck, H.-P. *J. Phys.: Condens. Matter* **1996**, *8*, 6465.
(59) Bradshaw, A. M.; Richardson, N. V.; Eds. *IUPAC, Pure Appl. Chem.* **1996**, *68*, 457.
(60) Klamroth, T.; Saalfrank, P.; Höfer, U. *Phys. Rev. B* **2001**, *64*, 035420.
(61) Jorgensen, S.; Ratner, M. A.; Mikkelsen, K. V. *J. Chem. Phys.* **2001**, *115*, 4314.
(62) Höfer, U.; Shumary, I. L.; Reuss, Ch.; Thomann, U.; Wallauer, W.; Fauster, Th. *Science* **1997**, *277*, 1480.
(63) Reuss, Ch.; Shumay, I. L.; Thomann, U.; Kutschera, M.; Weinelt, M.; Fauster, Th.; Höfer, U. *Phys. Rev. Lett.* **1998**, *82*, 153.
(64) Petek, H.; Ogawa, S. *Annu. Rev. Phys. Chem.* **2003**, *53*, 507.
(65) Gadzuk, J. W. *Phys. Rev. B* **1991**, *44*, 13466.
(66) Weik, F.; Meijere, A. de; Hasselbrink, E. *J. Chem. Phys.* **1993**, *99*, 682.
(67) Berglund, C. N.; Spicer, W. E. *Phys. Rev.* **1964**, *136*, A1030.
(68) Equation 16 has been modified from eq 30 of ref 33 by using the following relation: $\mathrm{Im}(\Sigma_{sub}) = -1/2i(\Sigma_{sub} - \Sigma^*_{sub}) = -1/2\Gamma_{sub}$.
(69) Datta, S. *Electronic Transport in Mesoscopic Systems*; Cambridge University Press: Cambridge, U.K., 2001; p 320.
(70) Sanvito, S.; Lambert, C. J. *Phys. Rev. B* **1999**, *59*, 11936.
(71) Krstic, P. S.; Zhang, X.-G.; Butler, W. H. *Phys. Rev. B* **2002**, *66*, 205319.
(72) Datta, S. *Nanotechnology* **2004**, *15*, S433.
(73) Taylor, J.; Gauo, H.; Wang, J. *Phys. Rev. B* **2001**, *63*, 245407.
(74) Xue, Y.; Datta, S.; Ratner, M. A. *Phys. Rev. B* **2002**, *281*, 151.
(75) Xue, Y.; Ratner, M. A. *Phys. Rev. B* **2004**, *69*, 085403.
(76) Kirchmann, P. S.; Loukakos, P. A.; Bovensiepen, U.; Wolf, M. *New J. Phys.* **2005**, *7*, 113.
(77) Wong, C. M.; McNeill, J. D.; Gaffney, K. J.; Ge, N.-H.; Miller, A. D.; Liu, S. H.; Harris, C. B. *J. Phys. Chem. B* **1999**, *103*, 282.
(78) Hotzel, A.; Wolf, M.; Gauyacq, J. P. *J. Phys. Chem. B* **2000**, *104*, 8438.
(79) Berthold, W.; Höfer, U.; Feulner, P.; Chulkov, E. V.; Silkin, V. M.; Echenique, P. M. *Phys. Rev. Lett.* **2002**, *88*, 056805.
(80) Ogawa, S.; Petek, H. *Surf. Sci.* **1996**, *357−358*, 585.
(81) Berthold, W.; Güdde, J.; Feulner, P.; Höfer, U. *Appl. Phys. B* **2001**, *73*, 865.
(82) Ryu, S.; Chang, J.; Kim, S. K. *J. Chem. Phys.* **2005**, *123*, 114710.
(83) Sarria, I.; Osma, J.; Chulkov, E. V.; Pitarke, J. M.; Echenique, P. M. *Phys. Rev. B* **1999**, *60*, 11795.
(84) Andres, P. de; Echenique, P. M.; Flores, F. *Phys. Rev. B* **1987**, *35*, 4529.
(85) Harris, S. M.; Holloway, S.; Darling, G. R. *J. Chem. Phys.* **1995**, *102*, 8235.
(86) Nitzan, A.; Ratner, M. A. *Science* **2003**, *300*, 1384.
(87) Marcus; R. A.; Sutin, N. *Biochim. Biophys. Acta* **1985**, *811*, 265.
(88) Ge, N.-H.; Wong, C. M.; Lingle, R. L., Jr.; McNeill, J. D.; Gaffney, K. J.; Harris, C. B. *Science* **1998**, *279*, 202.
(89) Gahl, C.; Bovensiepen, U.; Frischkorn, C.; Wolf, M. *Phys. Rev. Lett.* **2002**, *89*, 107402.
(90) Bovensiepen, U.; Gahl, C.; Wolf, M. *J. Phys. Chem. B* **2003**, *107*, 8706.
(91) Miller, A. D.; Bezel, I.; Gaffney, K. J.; Garrett-Roe, S.; Liu, S. H.; Szymanski, P.; Harris, C. B. *Science* **2002**, *297*, 1163.
(92) Onda, K.; Li, B.; Zhao, J.; Jordan, K.; Yang, J.; Petek, H. *Science* **2005**, *308*, 1154.
(93) Zhao, J.; Li, B.; Onda, K.; Feng, M.; Petek, H. *Chem. Rev.* **2006**, in press.
(94) Schenter, G. K.; Garrett, B. C.; Truhlar, D. A. *J. Phys. Chem. B* **2001**, *105*, 9672.
(95) Hertel, T.; Knoesel, E.; Wolf, M.; Ertl, G. *Phys. Rev. Lett.* **1996**, *76*, 535.
(96) Wolf, M.; Hotzel, A.; Knoesel, E.; Velic, D. *Phys. Rev. B* **1999**, *59*, 5926.

(97) Hertel, T.; Knoesel, E.; Hotzel, A.; Wolf, M.; Ertl, G. *J. Vac. Sci. Technol. A* **1997**, *15*, 1503.
(98) Boger, K.; Roth, M.; Weinelt, M.; Fauster, Th.; Reinhard, P.-G. *Phys. Rev. B* **2002**, *65*, 075104.
(99) Ramakrishna, S.; Willig, F.; Knorr, A. *Appl. Phys. A* **2004**, *78*, 247.
(100) Zeiser, A.; Büking, N.; Förstner, J.; Knorr, A. *Phys. Rev. B* **2005**, *71*, 245309.
(101) Hermanson, J. *Solid State Commun.* **1977**, *22*, 9.
(102) Gundlach, L.; Ernstorfer, R.; Riedle, E.; Eichberger, R.; Willig, F. *Appl. Phys. B* **2005**, *80*, 727.
(103) Kubo, A.; Onda, K.; Petek, H.; Sun, Z.; Jung, Y. S.; Kim, H. K. *Nanoletters* **2005**, *5*, 1123.
(104) Cinchetti, M.; Schönhenhense, G. *J. Phys.: Condens. Matter* **2005**, *17*, S1319.
(105) Bartels, L.; Meyer, G.; Rieder, K.-H.; Velic, D.; Knoesel, E.; Hotzel, A.; Wolf, M.; Ertl, G. *Phys. Rev. Lett.* **1998**, *80*, 2004.
(106) Guayacq, J. P.; Borisov, A. G.; Raşeev, G. *Surf. Sci.* **2001**, *490*, 99.
(107) Ogawa, S.; Nagano, H.; Petek, H. *Phys. Rev. Lett.* **1999**, *82*, 1931.
(108) Petek, H.; Weida, M. J.; Nagano, H.; Ogawa, S. *Surf. Sci.* **2000**, *451*, 22.
(109) Bauer, M.; Pawlik, S.; Aeschlimann, M. *Phys. Rev. B* **1999**, *60*, 5016.
(110) Borisov, A. G.; Kaznsky, A. K.; Guayacq, J. P. *Surf. Sci.* **1999**, *430*, 165.
(111) Borisov, A. G.; Guayacq, J. P.; Chulkov, E. V.; Silkin, V. M.; Echenique, P. M. *Phys. Rev. B* **2002**, *65*, 235434.
(112) Bauer, M.; Pawlik, S.; Burgermeister, R.; Aeschlimann, M. *Surf. Sci.* **1998**, *402*−*404*, 62.
(113) Dutton, G.; Zhu, X.-Y. *J. Phys. Chem. B* **2002**, *106*, 5975.
(114) Dutton, G.; Zhu, X.-Y. *J. Phys. Chem. B* **2004**, *108*, 7788.
(115) Dutton, G.; Quinn, D. P.; Lindstrom, C. D.; Zhu, X.-Y. *Phys. Rev. B* **2005**, *72*, 045441.
(116) Gahl, C.; Ishioka, K.; Zhong, Q.; Hotzel, A.; Wolf, M. *Faraday Discuss.* **2000**, *117*, 191.
(117) Machado, M.; Chulkov, E. V.; Silkin, V. M.; Hofer, U.; Echenique, P. M. *Prog. Surf. Sci.* **2003**, *74*, 219.
(118) Berthold, W.; Rebentrost, F.; Feulner, P.; Hofer, U. *Appl. Phys. A* **2004**, *78*, 131.
(119) Lingle, R. L., Jr.; Ge, N.-H.; Jordan, R. E.; McNeill, J. D.; Harris, C. B. *Chem. Phys.* **1996**, *205*, 191.
(120) Lindstrom, C. D.; Quinn, D.; Zhu, X.-Y. *J. Chem. Phys.* **2005**, *122*, 124714.
(121) Salomon, A.; Cahen, D.; Lindsay, S.; Tomfohr, J.; Engelkes, V. B.; Frisbie, C. D. *Adv. Mater.* **2003**, *15*, 1881.
(122) Vondrak, T.; Wang, H.; Winget, P.; Cramer, C. J.; Zhu, X.-Y. *J. Am. Chem. Soc.* **2000**, *122*, 4700.
(123) Miller, A. D.; Gaffney, K. J.; Liu, S. H.; Szymanski, P.; Garret-Roe, S.; Wong, C. M. *J. Phys. Chem. A* **2002**, *106*, 7636.
(124) Lindstrom, C. D.; Muntwiler, M.; Zhu, X.-Y. *J. Phys. Chem. B* **2005**, *109*, 21492.
(125) Muntwiler, M.; Lindstrom, C. D.; Zhu, X.-Y. *J. Chem. Phys.* **2006**, *124*, 081104.
(126) Lavrich, D. J.; Wetterer, S. M.; Bernasek, S. L.; Scoles, G. J. *J. Phys. Chem. B* **1998**, *102*, 3456.
(127) Perebeinos, V.; Newton, M. *Chem. Phys.* **2005**, *319*, 159.
(128) Rohleder, M.; Berthold, W.; Güdde, J.; Höfer, U. *Phys. Rev. Lett.* **2005**, *94*, 017401.
(129) Zhu, X.-Y.; Dutton, G.; Quinn, D. P.; Lindstrom, C. D.; Schultz, N. E.; Truhlar, D. G. Submitted to *Phys. Rev. Lett.*
(130) Lee, J.; Ryu, S.; Chang, J.; Kim, S.; Kim, S. K. *J. Phys. Chem. B* **2005**, *109*, 14481.
(131) Lee, J.; Ryu, S.; Ku, J. S.; Kim, S. K. *J. Chem. Phys.* **2001**, *115*, 10518.
(132) Lee, J.; Ryu, S.; Kim, S. K. *Surf. Sci.* **2001**, *481*, 163.
(133) Jacquemin, R.; Kraus, S.; Eberhardt, W. *Solid State Commun.* **1998**, *105*, 449.
(134) Link, S.; Scholl, A.; Jacquemin, R.; Eberhardt, W. *Solid State Commun.* **1998**, *113*, 689.
(135) Shipman, S. T.; Garrett-Roe, S.; Szymanski, P.; Yang, A.; Strader, M. L.; Harris, C. B. *J. Phys. Chem. B* **2006**, *110*, 10002.
(136) Vondrak, T.; Zhu, X.-Y. *J. Phys. Chem. B* **1999**, *103*, 3449.
(137) Brühwiler, P. A.; Karis, O.; Mårtensson, N. *Rev. Mod. Phys.* **2002**, *74*, 703.
(138) Bjorneholm, O.; Nilsson, A.; Sandell, A.; Hernnas, B.; Martensson, N. *Phys. Rev. Lett.* **1992**, *68*, 1892.
(139) Wurth, W.; Menzel, D. *Chem. Phys.* **2000**, *251*, 141.
(140) Schnadt, J.; Brühwiler, P. A.; Patthey, L.; O'Shea, J. N.; Södergren, S.; Odelius, M.; Ahuja, R.; Karis, O.; Bässler, M.; Persson, P.; Siegbahn, H.; Lunell, S.; Mårtensson, N. *Nature* **2002**, *418*, 620.
(141) Föhlisch, A.; Menzel, D.; Feulner, P.; Ecker, M.; Weimar, R.; Kostov, K. L.; Tyuliev, G.; Lizzit, S.; Larciprete, R.; Hennies, F.; Wurth, W. *Chem. Phys.* **2003**, *289*, 107.
(142) Föhlisch, A.; Feulner, P.; Hennies, F.; Fink, A.; Menzel, D.; Sanchez-Portal, D.; Echenqiue, P. M.; Wurth, W. *Nature* **2005**, *436*, 373.
(143) Dutton, G.; Zhu, X.-Y. *J. Phys. Chem. B* **2001**, *105*, 10912.
(144) Adams, D.; Brus, L.; Chidsey, C. E. D.; Creager, S.; Creutz, C.; Kagan, C. R.; Kamat, P. V.; Lieberman, M.; Lindsay, S.; Marcus, R. A.; Metzger, R. M.; Michel-Beyerle, M. E.; Miller, J. R.; Newton, M. D.; Rolison, D. R.; Sankey, O.; Schanze, K. S.; Yardley, J.; Zhu, X. *J. Phys. Chem. B* **2003**, *107*, 6668.
(145) Tsuei, K.-D.; Yuh, J.-Y.; Tzeng, C.-T.; Chu, R.-Y.; Chung, S.-C.; Tsang, K.-L. *Phys. Rev. B* **1997**, *56*, 15412.
(146) Hoogen Boom, B. W.; Hesper, R.; Tjeng, L. H.; Sawatzky, G. A. *Phys. Rev. B* **1998**, *57*, 11939.
(147) Lu, X.; Grobis, M.; Khoo, K. H.; Louie, S. G.; Crommie, M. F. *Phys. Rev. B* **2004**, *70*, 115418.
(148) Lindstrom, C. D. Ph.D. Thesis, University of Minnesota, Minneapolis, MN, 2006.
(149) Dudde, R.; Reihl, B.; Otto, A. *J. Chem. Phys.* **1990**, *92*, 3930.
(150) Szymanski, P.; Garret-Roe, S.; Harris, C. B. *Prog. Surf. Sci.* **2005**, *78*, 1.
(151) Bovensiepen, U. *Prog. Surf. Sci.* **2005**, *78*, 87.
(152) Liu, S. H.; Miller, A. D.; Gaffney, K. J.; Szymanski, P.; Garrett-Roe, S.; Bezel, I.; Harris, C. B. *J. Phys. Chem. B* **2002**, *106*, 12908.
(153) Stahler, J.; Gahl, C.; Bovensiepen, U.; Wolf, M. *J. Phys. Chem. B* **2006**, *110*, 9637.
(154) Gahl, C. et al. To be published.

CR0501689